Summer 2018

The Role of RAD4 in DNA Repair and Its Interplay with Telomeres in Tetrahymena thermophila

Emily Nischwitz
Missouri State University, Nischwitz017@live.missouristate.edu

THE ROLE OF RAD4 IN DNA REPAIR AND ITS INTERPLAY WITH TELOMERES IN TETRAHYMENA THERMOPHILA

A Masters Thesis

Presented to

The Graduate College of

Missouri State University

In Partial Fulfillment

Of the Requirements for the Degree

Master of Science Cell and Molecular Biology

By

Emily Nischwitz

August 2018

THE ROLE OF RAD4 IN DNA REPAIR AND ITS INTERPLAY WITH TELOMERES IN TETRAHYMENA THERMOPHILA

Biomedical Sciences

Missouri State University, August 2018

Master of Science in Cell and Molecular Biology

Emily Nischwitz

ABSTRACT

Telomeres are repetitive parts of the genome that act as a protective end cap to the chromosomes. Telomeres are critical to the integrity and stability of the genome, therefore, ensuring that their sequence is maintained, even after damage, is crucial. Much of the pioneering work responsible for explaining telomeres has been conducted in ciliates, specifically in *Tetrahymena thermophila*. Telomeres in *T. thermophila* have a high amount of tandem thymine repeats (GGGGTT) and, thus, are susceptible to ultraviolet light (UV) induced lesions called pyrimidine dimers, which must be repaired by nucleotide excision repair (NER). In humans, Xeroderma Pigmentosum C (XPC) is a protein that helps recognize DNA damage in NER. The *Tetrahymena thermophila* homolog to XPC (*RAD4*) showed strong evolutionary conservation to higher level eukaryotes making it an ideal model organism. *RAD4* expression was depleted by cloning and expressing a short hairpin RNA gene that will target RAD4. After both UV and hydrogen peroxide treatment, *Rad4* depleted cells had reduced survivability. Moreover, a DIG-labeled detection assay was developed for detection of telomere length, without the use of radioactivity. Telomere length increased in the absence of *Rad4* which reveals its role in telomere maintenance. This work ultimately provides two new resources to the fields of NER and telomeres by means of *Rad4* knockdown *T. thermophila* strains, and DIG-labeled telomere detection assay.

KEYWORDS: DNA repair, telomeres, *RAD4*, XPC, NER, *Tetrahymena thermophila*, DIG labeling

This abstract is approved as to form and content

_____

Dr. Joshua J. Smith
Chairperson, Advisory Committee
Missouri State University

THE ROLE OF RAD4 IN DNA REAPIR AND ITS INTERPLAY WITH TELOMERES IN TETRAHYMENA THERMOPHILA

By

Emily Nischwitz

A Masters Thesis
Submitted to the Graduate College
Of Missouri State University
In Partial Fulfillment of the Requirements
For the Degree of Master of Science in Cell and Molecular Biology

August 2018

Approved:

_____
Joshua J. Smith, PhD

_____
Randi J. Ulbricht, PhD

_____
Colette M. Witkowski, PhD

_____
Julie J. Masterson, PhD: Dean, Graduate College

ACKNOWLEDGEMENTS

I want to thank the entire Biomedical Sciences Department for their years of support. Each professor and staff member has made my education a fruitful and life changing endeavor. Thank you to the graduate college for thesis funding and support.

I would also like to acknowledge Dr. Benjamin Linger for his guidance and advice in the design of DIG labeled telomere detection system, and Dr. Wayne Mitchell for his assistance and guidance in the statistical analysis within this thesis. Also, a special thank you to the members of Smith Lab who have assisted in this project: Inyeong Lee, Taylor Walker, and Lynsie Daniels.

Additionally, each of my committee members has been invaluable. Dr. Smith's mentorship and guidance has made me into the scientist and person I am today. He has created an impression on me that will last a life time, and I am eternally grateful for all of the opportunities he has given me. Both Dr. Ulbricht and Dr. Witkowski have fostered such growth in me as both a scientist and writer, and specifically Dr. Ulbricht's advice both in regards to my project and life will be something I will take with me for years.

Without the support of my friends and family this would not have been possible. With all my love, I would like to thank my mother Maria Nischwitz and my father James Nischwitz for always encouraging and supporting me in the pursuit of my education and dreams.

TABLE OF CONTENTS

Introduction....1
- Telomeres....1
- Telomere and Telomerase Discovery....3
- Shelterin Proteins....5
- Telomere Proteins in *Tetrahymena thermophila*....8
- Telomere Dysregulation....9
- Nucleotide Excision Repair....11
- Nucleotide Excision Repair at the Telomeres....18
- Purpose Statement....19

Experimental Procedures....21
- Bioinformatics – Phylogenetic Tree Design and shRNA Primer Design....21
- shRNA Plasmid Construction....22
- Electroporation of DH10B *Escherichia coli* with pBT1-shRNA:RAD4....24
- Lysozyme Boil Plasmid Isolation and Ethanol Precipitation....24
- Restriction Enzyme Digest Confirmation of pBT1-shRNA:RAD4....25
- Linearization of pBT1-shRNA:RAD4 for Biolistic Transformation....26
- Cell Culture Maintenance and Strains Used....26
- Biolistic Transformation of *Tetrahymena thermophila*....27
- Knock Down Confirmation via Whole-Cell PCR....29
- Total RNA Isolations....30
- Quantitative Reverse Transcriptase Polymerase Chain Reaction (qRT-PCR)....31
- Survivability Assay of *Rad4* Knock Down Strains in *T. thermophila*....32
- *T. thermophila* Genomic DNA Isolation....32
- DIG-Labeled Telomere Probe Detection Assay....33
- Statistical Analysis....35

Results....36
- Conservation of Shelterin and XPC/RAD4 Proteins....36
- Quantification of *Tetrahymena thermophila RAD4* Expression Levels Before and After Damage....39
- Established *Rad4* Knock Down Strains in *T. thermophila*....45
- Verification of *Rad4* Knock Down Strains in *T. thermophila*....48
- Effect of UV and Hydrogen Peroxide on *Rad4* Knock Down Survivability....54
- Experimental Design and Optimization of DIG-labeled Telomere Probe Detection Assay....54
- Telomere Length in *Rad4* Knock Down Strain....63

Discussion....66
- The Role of *RAD4* in NER and BER....66
- *Rad4* Knock Down Reveals Important Role in NER and BER....67
- Development of a DIG-Labeled Telomere Probe Detection Assay....68

The Effect of *RAD4* on Telomeres....70
Future Directions....71

References....75

LIST OF TABLES

Table 1. Primer Sequences.....23

Table 2. *Tetrahymena thermophila* Strains.....28

Table 3. Shelterin Proteins InterPro Domain Analysis.....37

Table 4. XPC/Rad4 InterPro Domain Analysis.....38

LIST OF FIGURES

Figure 1. Telomere Structure and Associated Proteins....2

Figure 2. Shelterin Proteins....6

Figure 3. Nucleotide Excision Repair Pathway....12

Figure 4. Structure of XPC/RAD23B....15

Figure 5. Maximum Likelihood Phylogenetic Tree of XPC/Rad4....40

Figure 6. Quantification of *RAD4* Expression After Ultraviolet (UV) Treatment....42

Figure 7. Quantification of *RAD4* Expression After Hydrogen Peroxide (H_2O_2) Treatment....43

Figure 8. Quantification of *RAD4* Expression after Methyl Methanesulfonate (MMS) Treatment....44

Figure 9. *RAD4* Expression Quantification After Hydrogen Peroxide, Methyl Methanesulfonate, and Ultraviolet Light Treatment....46

Figure 10. Construction of pBT1-shRNA:RAD4....47

Figure 11. Digest of pBT1-shRNA:RAD4....49

Figure 12. Knock Down Confirmation via Whole-Cell PCR....50

Figure 13. Quantification of *RAD4* Expression in the *Rad4* Knock Down Strains....51

Figure 14. Quantification of *RAD4* Expression in Knock Down Strains....53

Figure 15. Effects of *Rad4* Knock Down on Survival After UV Treatment....55

Figure 16. Effects of *Rad4* Knock Down on Survival After H_2O_2 Treatment....56

Figure 17. Development and Optimization of DIG-Labeled Telomere Probe Detection Assay....58

Figure 18. Optimization of gDNA Isolations for DIG-Labeled Telomere Probe Detection Assay....59

Figure 19. Optimization of Blotting Conditions for DIG-Labeled Telomere Probe Detection Assay. 61

Figure 20. Telomere Detection in Wild Type and *Rad4* Knock Down Strains 62

Figure 21. Telomere Quantification in Wild Type and *Rad4* Knock Down Strains.....64

INTRODUCTION

Telomeres

Each cell in the human body contains approximately seven billion base pairs of deoxyribose nucleic acid (DNA) (Gillooly et al., 2015). This DNA contains all of the genetic information, and encodes all components of life (Watson and Crick, 1953). Genomic DNA is organized around a complex of proteins called histones that ultimately form nucleosomes that organize themselves into linear chromosomes. At the terminus of these chromosomes, there is a critical and unique structure called the telomere that is critical for the stability and integrity of the genome.

Both the sequence and structure of telomeres assist in genome protection (Figure 1A). Telomeric sequence across organisms is a simple sequence, repeated one hundred to one thousand times. The human telomeric repeat sequence is 5`-TTAGGG-3` (Moyzis et al., 1988). The sequence can vary, based on the organism, but it is typically G-rich which allows for the formation of G-quadruplexes. The formation of a G-quadraplex is stabilized based on the ability for guanines to bond to one another. This G-quandruplex has been hypothesized to play an important role in the capping and protecting function of telomeres (Henderson et al., 1987). Another unique component to the structure of telomeric sequence is the 3` single stranded G-rich overhang. This overhang is present due the inability of the replication machinery to fully replicate the linear chromosome to its terminus, leaving a shortened 5' end (Henderson and Blackburn, 1989). The 3` single stranded end of the telomere invades the upstream DNA duplex, base-pairing with the

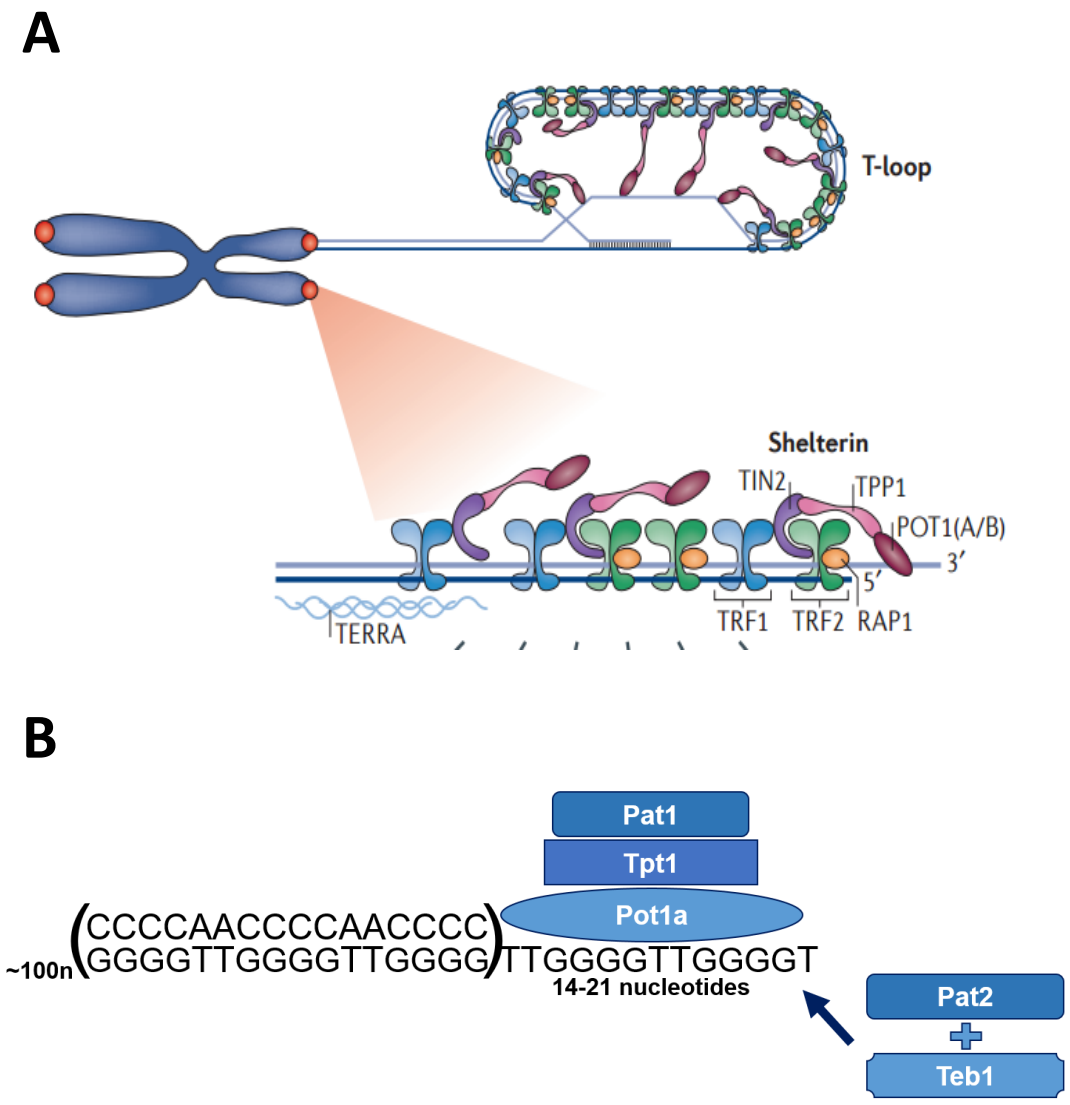

Figure 1. Telomere Structure and Associated Proteins. (A) Model of mammalian telomere structure and shelterin. The top of this figure shows the secondary structure that is created to protect its single stranded 3` overhang. The lower portion of the figure shows the six mammalian shelterin proteins (TRF1, TRF2, POT1, RAP1, TIN2, and TPP1) that associate with the telomeres to create the secondary structure and to further protect the ends of the chromosomes. (B) Model of *Tetrahymena thermophila* telomere structure and associated proteins. The sequence of *T. thermophila is* 5`-CCCCAA-3`, and it contains a 14-21 3` G-overhang. It is associated with the four shelterin-like proteins Pat1, Tpt1, Pot1a, and Pat2. Pat2 helps Teb1 (Telomerase in *T. thermophila*) associate with the telomere. (Adapted from Lazzerini-Denchi and Sfeir, 2016)

homologous telomere sequence and creating a structure called a T-loop (Griffith et al., 1999).

Telomeres have three widely conserved functions across organisms (Riethman, 2008). First, this sequence protects the ends of the chromosomes from degradation and being recognized as damage. Second, telomeres help organize chromosomes during meiosis to facilitate appropriate chromosome recombination and segregation (Bass et al., 1997). The third conserved function is reliant on the ability for the telomeric sequence to be extended by a ribonucleoprotein reverse transcriptase called telomerase (Greider and Blackburn, 1985). Without this unique DNA polymerase-independent extension mechanism, each round of replication would lead to telomere shortening, and threaten exposure of critical portions of the genome. Shortening of the telomeres will also lead to cellular senescence (Olovnikov, 1973).

Telomere and Telomerase Discovery

The discovery of telomeres and telomerase has a rich and collaborative history that involved a variety of model organisms and scientists. Originally theorized by McClintock, telomeres were named after their Latin origin telo (end) and mere (part) (McClintock, 1931; Mullner, 1938). Much of the pioneering work in telomere research has been conducted in the ciliate *Tetrahymena thermophila*. Due to its complex genome, it has a high number of chromosomes which in turn yields a large amount of telomeric DNA. Furthermore, this ciliate has nuclear dimorphism that splits the genetic information into a transcriptionally silent nucleus (micronucleus) and transcriptionally active nucleus (macronucleus) with 250 to 300 45N small chromosomes (Yao et al., 1981). Telomere

sequences specific to *T. thermophila* (5`-CCCCAA-3') are found at the end of chromosomes in the macronucleus and micronucleus (Blackburn and Gall, 1978). The macronuclear DNA of *T. thermophila* undergoes a fragmentation step which results in minichromosomes. These minichromsomes were observed to have telomeric sequence added to them, but the mechanism for the addition was unclear (Blackburn et al., 1983). The repetitive telomeric sequence was originally found on ribosomal DNA (rDNA), which is contained within approximately 9000 of minichromsomes (Figure 1; Yao et al., 1979).

Similar identification and characterization of telomeric sequence were found in a wide variety of ciliates (Katzen et al., 1981; Klobutcher et al., 1981; Boswell et al., 1982). Blackburn and Szostak studied the telomeric sequence of *Saccharomyces cerevisae* to ensure the translation of the original findings in *T. thermophila* and other ciliates translated to other organisms (Shampay et al., 1984). There are particular portions of the *S. cerevisae* genome that are circular, and highly unstable when linearized. Upon the experimental addition of the rDNA sequence from *T. thermophila* these linear segments were stable. This reinforced the hypothesis of the stabilizing properties of the telomeric sequence (Szostak and Blackburn, 1982).

Telomeric DNA is added to the termini of the telomeres of *T. thermophila* by a terminal transferase named telomerase. Because telomerase was first discovered in *Tetrahymena*, its telomerase is one of the best characterized telomerase ribonucleoprotein (Greider and Blackburn, 1985). Telomerase has two subunits that contribute to the functional structure; one is the RNA portion serving as a template sequence and the other is the catalytically active facilitating the addition of sequence. In 2009 Blackburn,

Greider, and Szostak were awarded the Nobel Prize in physiology or medicine for this discovery.

Telomerase functions in three main steps; binding, polymerization, and translocation (Riethman, 2008). It uses the 3`G-rich overhang to allow base pairing with the RNA subunit of telomerase called TERC (Telomerase RNA Component) in humans (Morin, 1989; Shippen-Lent and Blackburn, 1990). The RNA component contains complementary base pairs to the overhang, and positions the enzyme to the 3` OH. The 3'-OH of the telomere is then extended by the TERT (TElomerase Reverse Transcriptase) subunit of telomerase. This polymerization continues until the end of the RNA template. Telomerase translocates to the new 3` end or dissociates.

Shelterin Proteins

Proteins associated with the telomeres are essential in protecting and sheltering the telomeres from being detected by DNA surveillance proteins as DNA damage, and preventing DNA repair mechanisms recognizing the single strand of the telomeres and unnecessarily repairing this DNA (Palm and de Lange, 2008). This protective complex of proteins associated with telomeres is commonly referred to as shelterin. In mammals shelterin is a six protein complex, and each protein has unique functions that aid the telomere secondary structure (Figure 2A). These six proteins are TRF1, TRF2 (Telomere Repeat binding Factor 1 and 2), RAP1 (the human ortholog of the yeast Repressor/Activator Protein 1), TIN2 (Trf2- and Trf1-Interaction Nuclear protein), TPP1 (formerly known as Tint1, Ptop, or Pip1), and POT1 (Protection Of the Telomeres 1). TRF1 and TRF2 bind the double stranded portion of the telomeric sequence via their

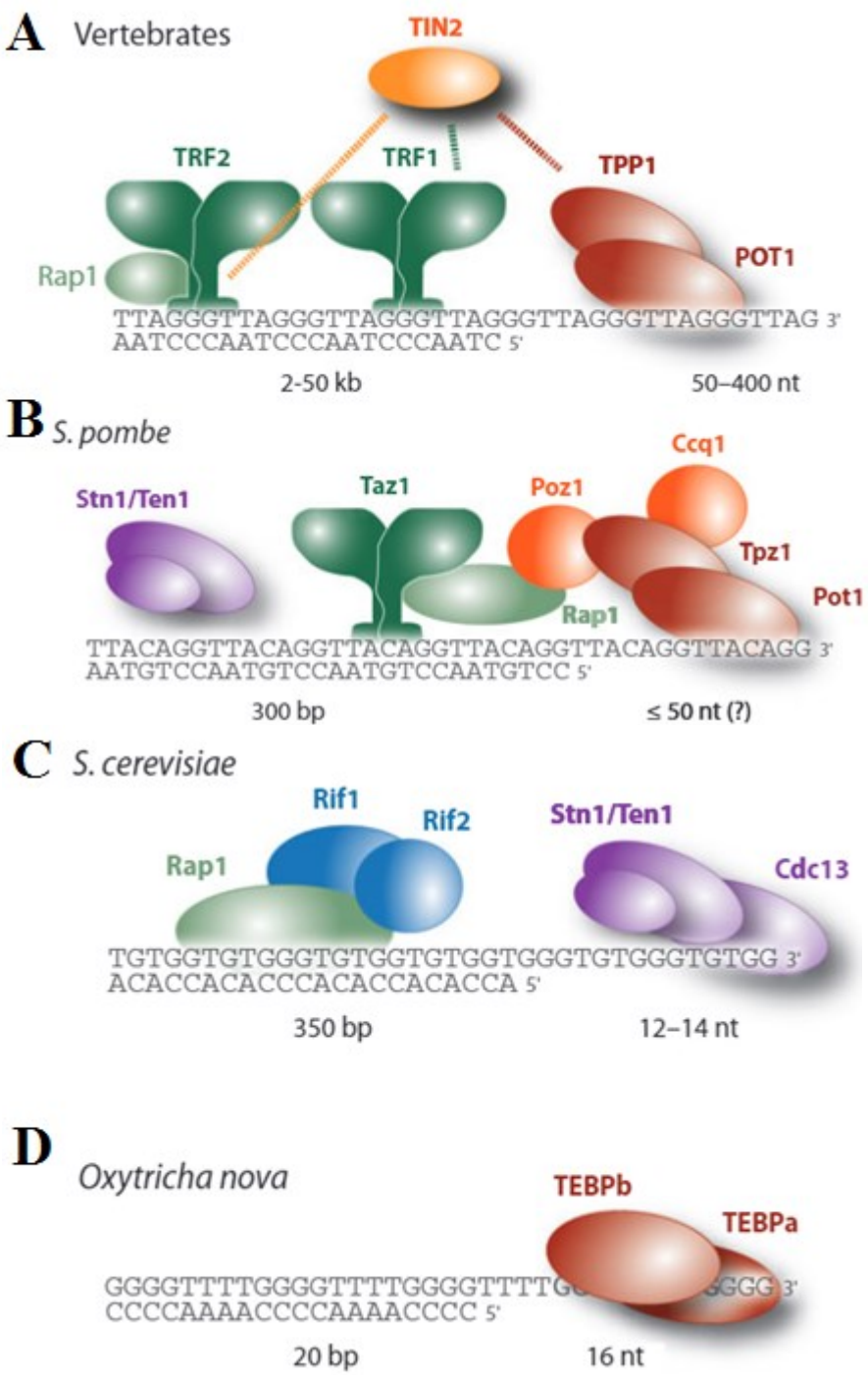

Figure 2. Shelterin Proteins. (A) The six shelterin proteins in vertebrates are POT1, RAP1, TIN2, TPP1, TRF1, and TRF2. (B) The six shelterin proteins in *Schizo-saccharomyces pombe* (*S. pombe*) are Ccq1, Pot1, Poz1, Rap1, Taz1, and Tpz1 with additional associated proteins Stn1 and Ten1. (C) The six shelterin proteins in *Saccharomyces cerevisase* (*S. cerevisiae*) are Cdc13, Rap1, Rif1, Rif2, Stn1, and Ten1. (D) The two shelterin proteins in *Oxytricha nova* are TEBPa and TEBPb (Palm and de Lange, 2008).

Myb binding motif, forming homodimers (Bianchi et al., 1997; Broccoli et al., 1997). RAP1 binds to TRF2 in the shelterin complex (Li et al., 2000). Without TRF2, RAP1 is highly unstable protein, and cannot localize to telomeric DNA (Celli and de Lange, 2005). TIN2 is a critical scaffold to the overall integrity of the shelterin complex, binding TRF1, TRF2, and TPP1 (Ye et al., 2004). TPP1 connects TIN2 and POT1, and is a direct positive regulator of telomerase activity (Xin et al., 2007). POT1 binds to the G-rich strand of the single stranded portion of the telomere, and protects it from degradation by nucleases (Lei et al., 2004). POT1 also functions as a negative regulator of telomerase activity (Kelleher et al., 2005). POT1 was initially identified due to its sequence homology to TEBP alpha and beta (Telomere End Binding protein alpha and beta) in *Oxytricha nova* (Figure 2D). Of the six shelterin proteins, it holds the highest amount of sequence similarity across model organisms (Baumann and Cech, 2001).

Schizosaccharomyces pombe has six shelterin proteins that have a very similar functional and structural architecture to vertebrate shelterin: Taz1 (Telomere-Associated in *Schizosaccharomyces pombe*), Rap1 (Repressor/Activator site binding Protein 1), Poz1 (Pot1-associated in *Schizosaccharomyces pombe*), Tpz1 (TPP1 homolog in *Schizosaccharomyces pombe)*, Ccq1 (Coiled-Coil protein Quantitatively enriched), and Pot1 (Protection of Telomeres 1) (Figure 2B). Taz1 has similar characteristics to TRF1/2, and binds double stranded telomere repeat as a homodimer (Cooper et al., 1997). Rap1 resembles the functionality of Rap1 and serves as a bridge from Taz1 to Poz1 (Kanoh and Ishikawa, 2001). Poz1, Tpz1, and Ccq1 serve as a bridge between Taz1 and Pot1. Ccq1 has been associated with regulation in meiotic division and plays a role in the recruitment of telomerase (Flory et al., 2004; Tomita and Cooper, 2008). Pot1 was originally

discovered is *S. pombe* due to its sequence homology to the previously discovered TEBP alpha and beta (Telomere End Binding Protein) in *Oxytricha nova*. This telomere protein in *S. pombe* also binds to 3` G overhang, and possess similar regulatory functions as POT1 in vertebrates (Baumann and Cech, 2001).

Although shelterin proteins typically do not have close sequence homology, shelterin complex of proteins in other organisms have shown to possess functional homology. In *Saccharomyces cerevisiae*, three proteins associate with the G-rich single stranded overhang: Cdc13 (Cell Division Cycle 13), Stn1 (Suppressor of cdc ThirteeN 1), and Ten1 (TElomeric Pathways with STn 1) (Gao et al., 2007) (Figure 2C). Cdc13 assists in the recruitment of telomerase, while Stn1 inhibits the binding of telomerase to the telomeres (Pennock et al., 2001; Puglisi et al., 2008). Rap1 (Repressor/ Activator site binding Protein 1) binds directly to the double stranded portion of the *S. cerevisae* telomere. Rap1 has the binding partners Rif1 and 2 (Rap1 Interaction Factor 1 and 2) which directly regulate telomere length (Marcand et al., 1997). As the binding of Rif1 and Rif2 increase association to Rap1, this complex inhibits the ability of telomerase to access the telomeres (Hirano et al., 2009).

Telomere Proteins in *Tetrahymena thermophila*

T. thermophila expresses four proteins that consistently associate with telomeric sequence and makes up its shelterin: Pot1a (protection of the telomeres 1a), Tpt1 (TPP1/Tpz1 in *Tetrahymena thermophila 1*), Pat1 (Pot1a associated *Tetrahymena thermophila* 1), and Pat2 (Pot1a associated *Tetrahymena thermophila* 2), (Figure 1B). Pot1a binds directly to the 3` overhand of the telomeres, and when knocked out has a

resulting phenotype of cell cycle arrest, telomere elongation, and an inability to protect the telomeres from degradation. It has also been implicated DNA damage surveillance, and overall cell signaling through ATM (ataxia-telangiectasia mutated) and ATR (ataxia telangiectasia and Rad3-related protein) (Jacob et al., 2007). Pot1b (later renamed Pot2) does not bind to telomeric DNA despite its extremely similar structure and sequence to Pot1a, but localizes to chromosomal breakage sites. Through chromatin immunoprecipitation analysis, Pot1b has been shown to have no interaction with other shelterin proteins (Cranert et al., 2014). Pot1a directly interacts with the single stranded DNA, and the shelterin proteins Tpt1 and Pat1. When Tpt1 expression is knocked down, longer telomeres are synthesized. Tpt1 has also been implication as a regulator in cell cycle checkpoint. Pat1 positively affects telomere length, but has no direct interaction with Tpt1 (Linger et. al., 2011). Pat2 is the main facilitator in telomerase telomere interaction. When Pat2 expression is knocked down, gradual shortening of telomeres occurs. Pat2 has not been demonstrated to interact directly with Pot1, Tpt1, or Pat1 (Premkumar et al., 2014).

Telomere Dysregulation

Telomeric dysregulation occurs when telomeres are lengthened, shortened, or their structure is perturbed. Dysregulation can be the result of both genetic changes and genotoxic stressors. Many times genetic changes can occur in the enzyme telomerase, leading to irregular sequence amount or content addition. Genetic changes can also cause differences in the shelterin protein composition. Improper association of shelterin to the telomeres can lead to aberrant telomere structure, and can also cause the dysregulation of

telomerase. Genotoxic stressors can damage the actual sequence of the DNA, causing single stranded or double stranded breaks, or lesions to individual bases.

Dysregulation that causes lengthened or shortened telomeres is associated with human disease and overall cellular dysfunction. One of the first diseases shown to be associated with short telomeres was dyskeratosis congenital due to a mutation in the transcriptional processing of telomerase. (Mitchell et al., 1999). Dyskeratosis patients have a higher propensity to develop cancer in comparison to the rest of the population (Alter et al., 2009). Shortened telomeres in all tissues are commonly associated with various types of lung diseases including pulmonary fibrosis and emphysema (Armanios, 2012; Stanley et al., 2015). These patients have an increased incidence of organ failure that accounts for about 90% of the deaths in this population (Dokal, 2000). Patients with longer telomeres are also predisposed to a variety of diseases including melanoma and glioma. Mutations in the POT1, TPP1, and RAP1 genes, which encode components of the shelterin complex, have also been associated with these types of cancers (Robles-Espinoza et al., 2014; 6, Kocak et al., 2014).

The inability to repair telomeric sequence after damage can also lead to aberrant telomeres. Because of the unique secondary structure and sequence of telomeres, damage is often processed differently at the telomeres in comparison to other parts of the genome. Typically, DNA repair machinery must interact with histones, but at the telomeres the repair machinery must also interact with shelterin proteins. An additional structural difference is the T-loop formed by the single stranded DNA invading upstream homologous double stranded DNA. Usually, DNA damage surveillance protein would recognize the single stranded 3’ end as DNA damage, but to maintain the integrity of the

telomere structure this should not be recognized as damage at this location of the genome.

If telomeres become critically short, this can induce non-homologous end joining. This is the only in the most dire of situations when cells are in distress. This can result in telomere-telomere fusions and ultimately overall genome instability (Stewart et al., 2012). Telomeres can also combat shortening through a telomerase independent method called alternative lengthening of the telomeres. Telomeric sequence undergoes homologous recombination of neighboring sequence to increase the overall length of the telomeres (Cesare and Reddel, 2010). Additionally, the three types of DNA excision repair (base excision repair, mismatch repair, and nucleotide excision repair) have been observed and studied at the telomeres (Jia et al., 2015). Nucleotide excision repair is particularly necessary because of the composition of telomere sequence, yet is understudied at this site of the genome.

Nucleotide Excision Repair

Nucleotide excision repair (NER) recognizes and repairs damage that occurs to a single strand of DNA due to physical and chemical mutagens in the environment and inside of the cell. UV light is a typical exogenous, physical mutagen that induces damage, generating both cyclobutane pyrimidine dimers (CPDs) and pyrimidine(6-4) pyrimidone photoproducts (6-4PP), that are repaired by NER (Figure 3). Adducts caused by environmental, chemical mutagens are benzo[α]pyrene and various aromatic amines, and are also repaired by NER (Szymkowski et al., 1993). All types of damage listed above typically have one major characteristic in common; interaction with DNA distorts the

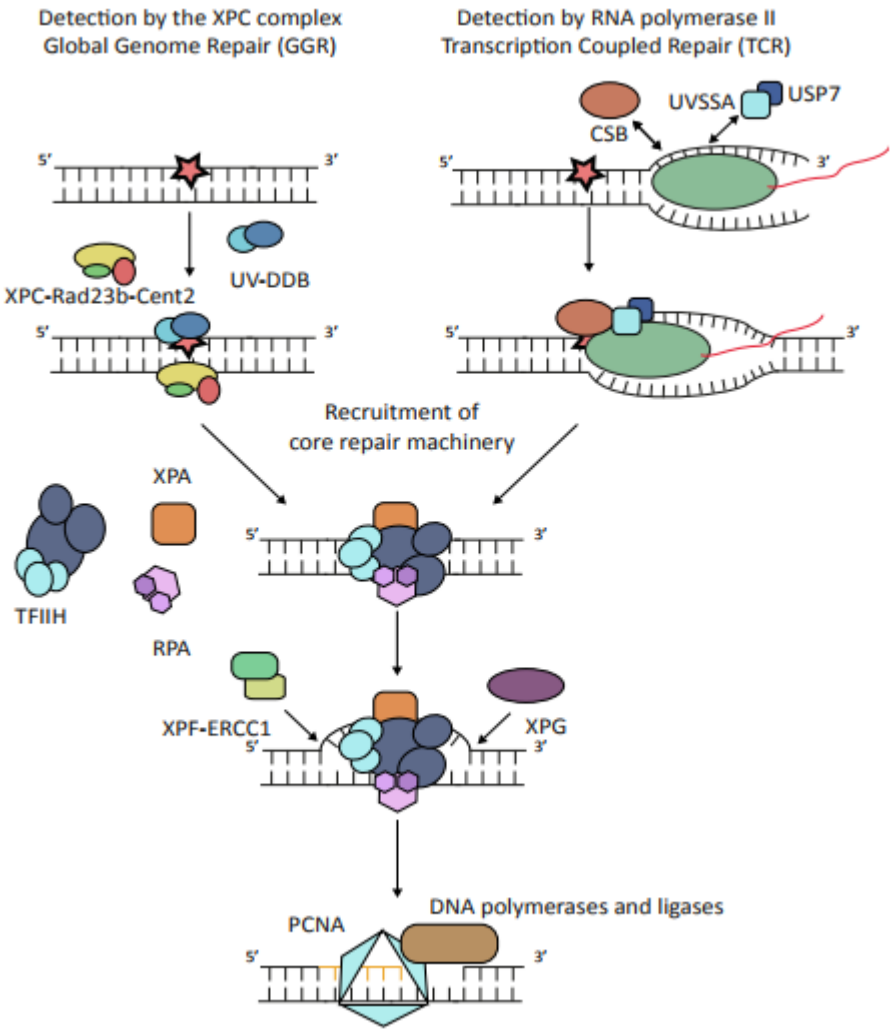

Figure 3. Nucleotide Excision Repair Pathway. The two nucleotide excision repair pathways are global genome NER (GGR; left) and transcription coupled NER (TCR; right). Global genome NER commences with the recognition of the damaged strand (shown with a red star) with the binding of XPC-Rad23b-Cent2 and UV-DDB. Transcription coupled NER starts with the stalling of RNA polymerase which signals the recruitment of CSB, UVSSA, and USP7. These two pathways converge and TFIIH, XPA, and RPA are recruited and unwind the helicase. XPF-ERCC1 and XPG make incisions on either side of the damage. The new strand is synthesized with DNA polymerase using the nondamaged strand as template, and sealed with ligase (van Belle, 2015).

double helix and thermodynamically destabilize DNA duplexes (Sugasawa et al., 2001). Because the recognition proteins in the NER pathway detect this helical distortion rather than the actual damaged base, NER is able to recognize a wide range of damage. This is a unique quality in comparison to other DNA damage repair pathways, which typically recognize the irregular structure and damage of the DNA. Along with this unique recognition characteristic, the discovery of the proteins within the NER pathway is different from other DNA repair pathways. Many of the proteins within the nucleotide excision repair pathway were discovered through studies of patients with Xeroderma Pigmentosum.

Xeroderma Pigmentosum patients cannot perform nucleotide excision repair (NER) due to a lack of one of the XP repair proteins. Researchers study these patients to better understand the overall pathway of NER and the pathobiology of Xeroderma Pigmentosum both clinically and through cellular culture (Cleaver, 1968). The hallmark phenotypic characteristic of this genetic disorder is extreme sensitivity to sunlight. Patients can have over a 2000-fold increase in the risk of skin cancer (DiGiovanna and Kramer, 2012). Many times, patients also have developmental delay, neurological damage, and overall increased risk of cancer (Cleaver, 2005). This phenotypic manifestation is likely due to the accumulation of DNA damage due to the inability for the damage to either be recognized or repaired by NER. In addition to Xeroderma Pigmentosum, mutations in various specific XP proteins can lead to Cockayne syndrome and trichothiodystrophy (Lehmann, 2003). Studies with XP patients have made great headway into understanding the NER pathway.

There are two types of nucleotide excision repair processes: global genome and transcription coupled repair. Transcription coupled repair as the name implies, focuses on repairing genes undergoing active transcription (Hanawalt and Spivak, 2008). Global genome repair is responsible for repairing both transcriptionally active and inactive parts of the genome (Gillet and Schärer, 2006). The primary difference between these two types of repair is the damage recognition step. Transcription coupled repaired responds largely to the RNA polymerase stalled at a site of damage in an actively transcribed portion of the genome (Figure 3; TCR pathway). The recognition factors specific to TCR are CSB (Cockayne Syndrome group B), UVSSA (UV-Stimulated Scaffold protein A), and USP7 (Ubiquitin-Specific-Processing protease 7).

Global genome repair begins with specific recognition factors of XPC-RAD23B (Xeroderma Pigmentosum C, RADiation sensitive 23B) and if necessary UV-DDB (Ultraviolet-Damaged DNA B) that recognize thermodynamically destabilized duplexes (Evans et al., 1997; Sugasawa et al., 2001) (Figure 3 GGR pathway). XPC, known as RAD4 (RADiation sensitive 4) in both yeast and *Tetrahymena thermophila,* contains two key functional domains: transglutamase homology domain (TGD) and Beta-hairpin domains 1-3 (BHD 1-3) (Figure 4). Both TGD and BHD1 anchor XPC and RAD23 to the DNA at the site of damage. BHD2 and 3 bind the undamaged strand encircling the two nucleotides across from the damage. This ability to bind the undamaged strand allows XPC-RAD23B to recognize a large variety of DNA damages (Min and Pavletich, 2007). While the domains of XPC assist in physically binding DNA, the main function of a large amount of helical destabilization. The recognition of CPD damage is facilitated by UV-DDB complex (Tang et al., 2000). DDB2 creates a significant kink in the DNA duplex,

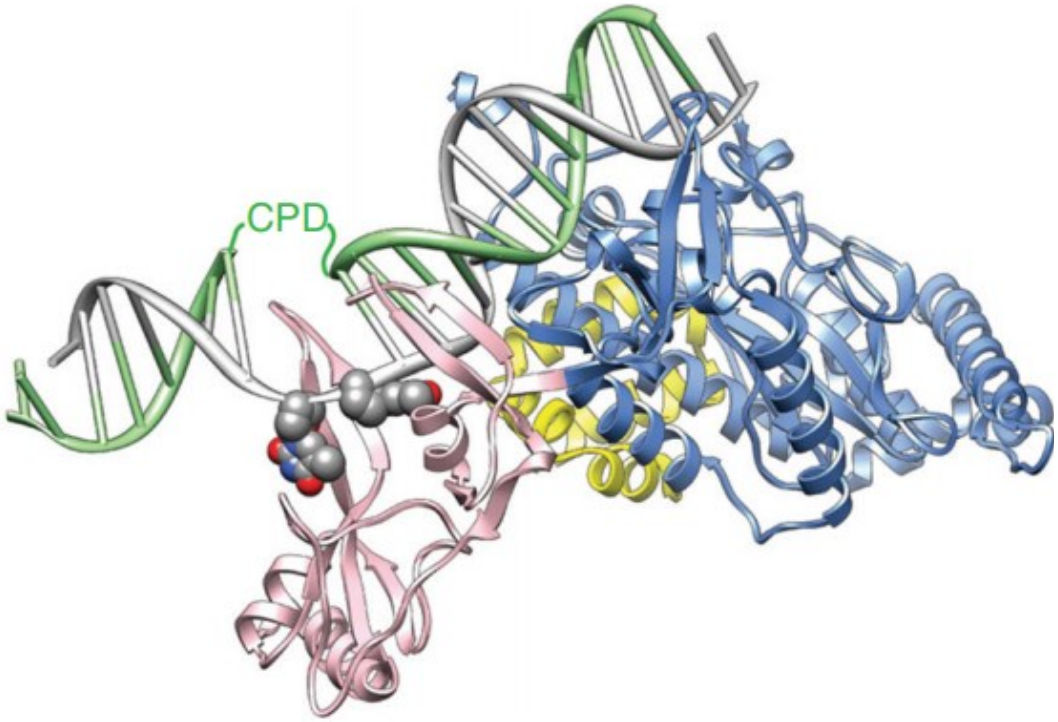

Figure 4. Structure of XPC/RAD23B. Ribbon diagram of XPC (pink and blue) and a portion of RAD23B (yellow). XPC is binding the strand opposite of the damage. The blue strand is the transglutaminase and beta hair pin 1 domain. The pink strand is the beta hair pin 2 and 3 domain (Schärer, 2013).

and this distortion is more recognizable to XPC-RAD23B (Scrima et al., 2008).

For both global and transcription coupled NER, the pathways converge once the damage is recognized, and initial protein complexes are stabilized. The next step required is the recruitment of the pre-incision complex. The pre-incision initiates with TFIIH, which is recruited to the site of damage by the presence of the recognition proteins. The TFIIH complex has a total of 10 subunits, with its catalytic proteins XPB and XPD which perform helicase activity (Evans, 1997; Tapias et al., 2004). The XPB functions to pry open the DNA duplex with the facilitation of XPC that allows loading of THIIH (Coin et al., 2008). XPD translocates along the single stranded DNA opening it, and stalls at the location of the damage (Sugasawa et al., 2009). This stalling causes the rest of the pre-incision complex to assemble, which includes XPA, RPA, and XPG; (Wakasugi and Sancar, 1998; Volker et al., 2001). Once these proteins are recruited the XPC-RAD23B complex dissociates, XPA then plays a key role in the placement and positioning of many of the nucleotide excision repair proteins including ERCC1-XPF, TFIIH, XPC-RAD23B complex, DDB2, and PCNA (Li et al., 1994; Park et al., 1995; Bunick et al., 2006; Wakasugi et al., 2009; Gilljam et al., 2012). RPA binds to and coats the ssDNA on the opposite side of the damage for a span of about 30 nucleotides, which is about the size of the damaged strand that will be removed (Fan and Pavletich, 2012). The placement of the RPA proteins helps to position ERCC1-XPF and XPG to allow for a dual incision to remove the damaged sequence (de Laat et al., 1998). ERCC1-XPF are recruited to this complex via XPA, and creates the first incision at the 5` end of the sequence (Li et al., 1994). This first incision is required at the 5` end before the second incision can be performed. XPG will only bind when a ssDNA stretch at the 3` end is present which is

created by this first incision (Hohl et al., 2003). The second incision at the 3` end is made by XPG (Fagbemi et al., 2011).

The incision made by ERCC1-XPF create a 3` hydroxyl group that can be used by DNA polymerase to fill in the gap created. There are three polymerases that have been associated with NER: Polymerase κ, Ɛ, and δ. Pol κ which is typically associated with translesion synthesis has been shown to be involved in NER (Ogi and Lehmann, 2006). When Pol Ɛ and δ expression is knocked down, there is a 50% reduction of repair synthesis. Each polymerase has specific proteins that facilitate the polymerase association to the DNA strand (Ogi et al., 2010). The 5` phosphate created by XPG will be ligated to the newly extended DNA fragment by DNA ligase I or DNA ligase IIIα to seal the backbone. DNA ligase IIIα is active in both dormant and actively replicating cells, while DNA ligase I is active in replicating cells (Moser et al., 2007).

Once the DNA has been successfully repaired, NER proteins dissociate, and the cell is able to resume its regular function. This is critical to both actively transcribed and silent portions of the genome. If NER does not occur in areas that are being actively transcribed this could lead to a point mutation, or the inability of RNA polymerase to be able to transcribe the gene successfully. In silent portions of the genome, this repair is critical because remaining damage could be passed to the next generation of cells. These mutations can cause phenotypic difference and overall genome instability. One silent portion of the gnome that is critical to genome stability is the telomeres. NER is important to maintain telomeric DNA, but thus far has been understudied.

Nucleotide Excision Repair at the Telomeres

Limited studies have been conducted with nucleotide excision repair at the telomeres. CPDs occur seven-fold higher at telomeres than the bulk genome in human fibroblast cells (Rochette and Brash, 2010). CPDs are removed 1.5-fold faster at the telomeres over genomic DNA, suggesting that NER at the telomeres is unique and efficient (Parikh et al., 2015). However, contradictory data has been published currently call into question if repair is due to nucleotide excision repair pathways or to other repair pathways (Parikh et al., 2015; Rochette and Brash, 2010). For example, primary mouse fibroblasts deficient in XPB and chronically exposed to low amounts of hydrogen peroxide, an agent that induces base excision repair (BER), have shorter telomeres and higher amounts of telomere degradation (Ting et al., 2010). A similar phenotype has been observed in XPB/XPD deficient lymphoblastoids treated with hydrogen peroxide (Gopalakrishnan et al., 2010). It is possible that these BER-related phenotypes may actually be related to NER since NER proteins can play a role in the BER pathway (Melis et al., 2013).

NER proteins are also directly involved in telomere maintenance via shelterin. XPF and the shelterin protein TRF2 have an intricate interaction; when XPF is over expressed, shorter telomere fragments occur, and less TRF2 interaction with the telomere is observed (Wu et al., 2008). Additionally, ERCC1/XPF is one of the endonucleases responsible for removing the 3` overhang of telomeres if left uncapped. TRF2 serves as the protector against the ERCC1/XPF endonuclease activity in regularly capped telomeres (Zhu et al., 2003).

NER proteins may also help regulate telomerase itself. $Xpc^{-/-}$ knock out *Mus musculus* have chronically longer telomeres, while double knock out *M. musculus* of Xpc and Terc (catalytic subunit of telomerase) show lengthened telomeres. This surprising lengthening of telomeres with the $Xpc^{-/-}$G1-$G3^{-/-}$ is likely due to alternative lengthening of the telomeres (ALT) (Stout and Blasco, 2013).

Currently, still much about the UV response and XPC activity at the telomere is unknown. Due to the unique structure, sequence, and critical role of telomeres (Figure 1), it is likely that the repair pathways are very individualistic to this part of the genome in comparison to typical genomic sequence. Thus far no nucleotide repair studies at the telomere have ever been conducted in *Tetrahymena thermophila* but it is an extremely well characterized model organism in telomere biology studies, and will allow DNA repair at this are of the genome to be addressed.

Purpose Statement

The major goal of this research project was to understand the behavior of RAD4, the homolog of XPC in *T. thermophila*, both generally in the genome as well as at the telomeres. RAD4 is a critical DNA damage recognition protein in the nucleotide excision repair pathway in the global genome pathway. The process of nucleotide excision repair at the telomeres is not well known, yet is intriguing because of the telomeres unique architecture and sequence. The telomere sequence in *T. thermophila* (3`-GGGGTT-5`) is especially prone to UV damage due to the frequency of thymine dinucleotides that may undergo UV-induced dimerization, which is typically repaired by nucleotide excision repair. Similarly, the mammalian telomeric sequence (TTAGGG) is also susceptible to

damage repaired by NER due to its dipyrimidine sequence. Thus, the integrity of telomeres may be affected if the nucleotide excision repair pathway is disrupted.

To begin these studies, *XPC* and *RAD4* sequences were analyzed by a variety of bioinformatics tools to define their homology. *RAD4* expression levels were observed after *T. thermophila* exposure to mutagens, including UV, hydrogen peroxide, and MMS, to induce DNA damage recognized and repaired by nucleotide excision repair, base excision repair, and double stranded break repair, respectively. To further characterize RAD4, a *RAD4* knock down was established via short hairpin RNA. Cellular growth after UV light and hydrogen peroxide exposure was measured to determine how RAD4 depletion affects the ability to recognize damaged DNA. Finally, telomere length and integrity were measured in the wild type and RAD4 depleted cells, before and after UV treatment via a unique DIG-labeled probe telomere detection assay. It was anticipated that the nucleotide excision repair pathway will be further characterized in the model organism, *T. thermophila*, providing further understanding of how nucleotide excision repair helps to maintain telomeres.

EXPERIMENTAL PROCEDURES

Bioinformatics – Phylogenetic Tree Design and shRNA Primer Design

RAD4 nucleotide sequence, amino acid sequence, exon and intron predictions, and paralogs were collected from Tetrahymena Genome Database (TGD; Stover et al., 2012). The paralog obtained from TGD was *RAD4* (TTHERM_00825460; Altschul et al., 1997). Orthologs were obtained using National Center for Biotechnology Information Basic Local Alignment Search Tool (NCBI BLAST; Altschul et al., 1997) search from *RAD4.* The following proteins were obtained as the top ortholog hits: NP_001460.1 (*Homo sapiens*), NP_034377.2 (*Mus musculus*), ABI54461.1 (*Danio rerio*), BAA76953.1 (*Xenopus laevis*), NP_504491.1 (*Caenorhabditis elegans*), AGA18917.1 (*Drosophila melanogaster*), XP_637925.1 (*Dictyostelium discoideum)*, AJS88329.1 (*Saccharomyces cerevisiae*), NP_587828.1 (*Schizosaccharomyces pombe*) NP_564012.1 (*Arabidopsis thaliana*), XP_002267875.1 (*Vitis vinifera*), and ABN13872.1 (*Aspergillus niger*).

Domain analysis was performed on these amino acid sequences with InterPro (Finn et al., 2017). Additionally, sequences were analyzed for evolutionary conservation with Multiple Sequence Alignment-CLUSTALW (Li et al., 2015), and Molecular Evolutionary Genetic Analysis 7.0 (MEGA7; Kumar et al., 2016). MEGA 7.0 was used to create a maximum likelihood tree using bootstrap consensus with 500 replicates. Sequences were analyzed with Tree-based Consistency Objective Function For alignment Evaluation (TCOFFEE; Notredame et al., 2000) to determine the appropriate location for knock down primer design (data not shown). Primers (shRNA) were analyzed using Integrate DNA Technologies OligoAnalyzer 3.1 (https://www.idtdna.com/calc/analyzer).

Domain analysis was performed on the shelterin proteins with InterPro of *Homo sapiens, Saccharomyces cerevisiae, Schizosaccharomyces pombe,* and *Tetrahymena thermophila.* The following proteins were analyzed for *Homo sapiens:* POT1 (NP_056265.2), RAP1 (ABA64473.1), TIN2 (AAF18439.1), TPP1 (NP_001075955.1) TRF1 (NP_059523.2), and TRF2 (NP_059523.2); *Saccharomyces cerevisiae*: CDC13 (NP_010061.1), RAP1 (NP_014183.1), RIF1 (NP_009834.4), RIF2 (NP_013558.3); *Schizosaccharomyces pombe*: CCQ1 (NP_588210.1), POT1 (NP_594453.1), POZ1 (NP_594428.1), RAP1 (NP_596285.1), TAZ1 (NP_594047.1), and TPZ1 (NP_001342857.1); *Tetrahymena thermophila:* POT1 (TTHERM_000378989), TPT1 (TTHERM_00523050), PAT1 (TTHERM_00013120), and PAT2 (TTHERM_00049470).

shRNA Plasmid Construction

The appropriate pBT1-YFG vector (from the work of Kyle Cottrell in 2012) was combined with the specific *RAD4* sense and antisense primers to construct a theoretical plasmid with Gene Construction Kit 3.0 (textco biosoftware). To phosphorylate the shRNA oligos, 200 pmol of the sense and antisense RAD4 oligos (Table 1), 10 units of T4-PNK (New England Biolabs), 1X PNK buffer (New England Biolabs), and 1 mM ATP were combined and brought to a final volume of 50 µL. The reaction was incubated at 37°C for 60 minutes, and then 70°C for ten minutes, 10 µL of this phosphorylation reaction was combined with 1XSSC and brought to a final volume of 25 µL. To anneal these oligos, this reaction was heated at 75°C for five minutes, and cooled in a 23°C

Table 1. **Primer Sequences.**

Target	Primer Sequence (5` to 3`)
ACT1	Forward: TGAATTAAAGGCTTACAAGGAATC
	Reverse: CACACTTCATGATAGAGTTGAAGG
DIG-ACT1	/5DigN/TGAATTAAAGGCTTACAAGGAATC
DIG-Telomere	/5DigN/CCCCAACCCCAACCCCAACCCCAACCCCAA
HHP1	Forward: TTAGCAATGATAAACCTTAGAC
	Reverse: TGTGTAAAGAGATTTTCCATC
RAD4 qRT-PCR	Forward: AGAGCTGCACGTTTTTCAGATATG (1032F)
	Reverse: TGACAGCATTTGGTCAAATAAATCA (1271R)
shRNA	Forward: ATGAATGATATAAATGAAGAGTGGC
Confirmation	Reverse: TGTTATGTGAATGAAGTTAATTGGG

annealed RAD4 oligos at 1:5 and 2:5 (vector:insert) molar ratios. These ligation reactions contained 1X T4 DNA ligase buffer (New England Biolabs) and 400 units T4 DNA ligase (New England Biolabs). Ligation reactions were incubated at 14°C overnight, and kept in at -20°C for long term storage.

Electroporation of DH10B *Escherichia coli* with pBT1-shRNA:RAD4

DH10B E. coli cells were combined with 1 µL of the pBT1-RAD4shRNA ligation reaction, and transferred to a 2-mm electroporation cuvette (Fisher) taking care to avoid the introduction of any bubbles. Samples were placed in the electroporation chamber (Bio-Rad Gene Pulser II Electroporation System) and electroporated at 2.5kV, 200 ohms, 25 µF. Samples were recovered in 1 mL of SOC media (Invitrogen) at 37°C for 60 minutes, and 100 µL of each sample was plated on a LB+AMP plates (1% bacto tryptone, 0.5% yeast extract, 1% NaCl, 1.5% bacterial agar with 100 µg/µL ampicillin), and incubated at 37°C for 12-20 hours.

Lysozyme Boil Plasmid Isolation and Ethanol Precipitation

Plasmid-containing bacteria were grown on LB+AMP plates (1% bacto tryptone, 0.5% yeast extract, 1% NaCl, 1.5% bacterial agar with 100 µg/µL ampicillin). Two milliliter (miniprep) and 25 mL (midiprep) cultures were grown in LB+AMP liquid media (1% bacto tryptone, 0.5% yeast extract, 1% NaCl, with 100 µg/µL ampicillin), and incubated overnight at 37°C in at 220 rpm. Cultures were centrifuged for two minutes (Sorvall Legend X1 Centrifuge, Thermo Fisher Scientific) at 13300 rpm (miniprep) or 6000 rpm (midiprep) for ten minutes. The remaining media was removed. Cellular pellet

was resuspended in 350 µL or 3.5 mL sucrose lysis buffer (8% sucrose, 0.5% Trion X-100, 50 mM EDTA, 10 mM Tris-pH 8) and 10 mg/mL lysozyme (Fisher Scientific). Samples were transferred to 1.5 mL microcentrifuge tubes, incubated at room temperature for five minutes, and boiled for one minute. Samples were spun at maximum speed for 15 minutes, and cellular debris was removed. To precipitate DNA, 220 µL of isopropanol and 40 µL 3 M sodium acetate were added and incubated for five minutes. Plasmid isolates were spun at maximum speed for 5 minutes, and washed with 70% ethanol. Samples were combined and resuspended in 50 µL (miniprep) or 300 µL (midiprep) TE (10 mM Tris-HCl, 1 mM EDTA-pH 8).

Midipreps were incubated with 10 mg/mL RNase A (AppliChem Panreac) at 37°C for 3 hours. Samples then underwent a phenol chloroform extraction. Purified samples were combined with $1/10^{th}$ 3 M sodium acetate and 2.5 times 100% chilled ethanol, and incubated at -20°C overnight. Samples were centrifuged at maximum speed for 10 minutes and the supernatant was poured off. The pellet was washed with 70% ethanol, and centrifuged for 10 minutes at maximum speed. The supernatant was discarded, and carefully removed. The plasmid was resuspended in 150 µL double distilled water.

Restriction Enzyme Digest Confirmation of pBT1-shRNA:RAD4

The isolated plasmid was digested with *SacI* (New England Biolabs) and *XhoI* (New England Biolabs) overnight at 37°C. Samples were electrophoresed on a 1.0% agarose gel in TAE at 120V for 30 minutes, and visualized with the KODAK Gel Logic 200 Imaging System. The strain considered positive for pBT1-shRNA:RAD4 after

analysis was grown up in a 2 mL culture in LB+AMP liquid media (1% bacto tryptone, 0.5% yeast extract, 1% NaCl, with 100 µg/µL ampicillin). For long term storage, glycerol stocks were made by combining culture and 10% glycerol in a 1:1 ratio, and stored at -80°C.

Linearization of pBT1-shRNA:RAD4 for Biolistic Transformation

Gene Construction Kit 3.0 was used find the best restriction enzymes to linearize the knock down plasmid after the *E. coli* transformation. A 200 µL sample was prepared with 1X SmartCut Buffer (NEB), 2.5 µL *XhoI*, 2.5 µL *SacI*, and 100 µg plasmid DNA and incubated over night at 37°C. The sample was centrifuged at maximum speed for 15 minutes. The precipitate was washed with 70% ethanol, and centrifuged for five minutes. Ethanol was removed, and sample was allowed to dry at room temperature. Sample was quantified on the NanoDrop spectrometer (NanoDrop 2000 Spectrophotometer, Thermo Fisher Scientific), and sample was adjusted to 2.0 µg/µL in water. One µL sample was run on a 1.0% agarose gel in TAE at 120V for 30 minutes, and visualized with the KODAK Gel Logic 200 Imaging System to ensure proper digestion sizes before biolistic transformation.

Cell Culture Maintenance and Strains Used

Tetrahymena thermophila were grown in 2% PPY media (0.02 g/mL protease peptone, 0.002 g/mL yeast extract) and 1XPSF (100 µg/mL penicillin, 100 µg/mL streptomycin, 0.25 µg/mL amphotericin B, Thermo Fisher Scientific). Cultures grown in plates (96-, 48-, and 24-well plates) were incubated in humidity chambers at 30°C.

Cultures grown in larger quantities for RNA isolation, survivability assay, gDNA isolations, and any other experiments were grown at 30°C at 100 rpm. Concentrations of cells throughout experimentation were estimated via a hemocytometer. Stock cultures were either continued or established in 1% PPY+10 mM Tris and 1XPSF. Stock cultures were maintained approximately every 4-6 months by transferring 100 µL of the original stock to a new 1% PPY+10 mM Tris and 1XPSF. All strains used during the course of this project are described in Table 2. Strains designated with a "CU" indicate that the strain was obtained from the Tetrahymena Stock Center located at Cornell University.

Biolistic Transformation of *Tetrahymena thermophila*

The gold beads were prepared by weighing out 30 mg of Au particles, and 70% ethanol was added. The beads were vortexed for three to five minutes, centrifuged at maximum speed for five seconds and the supernatant was discarded. These steps were repeated three times.

To prepare the cells, a culture was started by inoculating 25 mL culture of 2% PPY media (0.02 g/mL protease peptone, 0.002 g/mL yeast extract and 1XPSF (100 µg/mL penicillin, 100 µg/mL streptomycin, 0.25 µg/mL amphotericin B, Thermo Fisher Scientific) culture with a 0.5 mL of stock culture of either CU428, CU522, or CU725 (Table 2). The next day a culture was diluted to a final concentration of 1 to $3x10^5$cell/mL at the time of the transformation. The next day the culture was centrifuged at 3000 rpm for three minutes (Sorvall Legend X1 Centrifuge, Thermo Fisher Scientific). The supernatant was decantated and the pellet resuspended in 10 mM Tris and

Table 2. *Tetrahymena thermophila* Strains.

Name	Genotype	Phenotype	Description
CU428	*MIC: mrp1-1/mrp1-1*	6-methylpurine resistance	Used as wild type strain in all experimentation unless otherwise stated
CU522	*MIC: mpr1-1/mpr1-1, btu1-1::btu1-1M350K/btu1-1::btu1-1M350K.* *MAC: btu1-1::btu1-1M350K*	Paclitaxel sensitive Vinblastine resistant	*BTU1* mutant used for transformation of knock down constructs
CU725	*MIC: chx1-1/chx1-1 btu1-1::btu1-1M350K/btu1-1::btu1-1M350K* *MAC: btu1-1::btu1-1M350K*	Cyclohexamide, paclitaxel sensitive, vinblastine resistant	*BTU1* mutant used for transformation of knock down constructs
shRNA *RAD4* (Clone 1, Clone 10)	*MAC: btu1-1M350K :: shRNA-RAD4*	Paclitaxel resistance	Knockdown of *RAD4* by short-hairpin RNA, recombined in *BTU1* locus, Modification of CU522
shRNA *RAD4* (Clone 11)	*MAC: btu1-1M350K :: shRNA-RAD4*	Paclitaxel resistance	Knockdown of *RAD4* by short-hairpin RNA, recombined in *BTU1* locus, Modification of CU725

centrifuged again for 3 minutes. The 10 mM Tris was decanted, and the cell pellet was resuspended in 10 mM Tris pH. Cultures were then placed in 30°C without shaking for 14 to 20 hours. Media was pre-warmed at 30°C for transformations.

The gold beads had 5 µg of the linearized knock down plasmid, 25 µL 2.5 M calcium chloride, and 10 µL 100 mM spermidine added. The mixture was vortexed for 30 minutes at 4°C. The mixture was centrifuged, the supernatant was removed, and 70% ethanol was added; this was repeated with 100% ethanol. The steel macrocarrier holder, plastic macrocarrier, plastic cap, and metal stopping screens were sterilized by dipping in 100% ethanol. The rupture disks were sterilized by dipping in 100% isopropanol.

Prepared gold samples were added to the macrocarrier. Ten mM HEPES was placed on a filter and $1x10^7$ of cells were added. The gene gun (Bio-Rad PDS-1000/HeTM Biolistic Particle Delivery System) was set up the as follows: rupture disk (1100 PSI for 900 PSI) has a 3/8 inch gap to the macrocarrier assembly,stopping screen was in the third position, and was placed in the macrocarrier assembly, and cell plate station was in the bottom most position. The vacuum pump was turned on and a vacuum was created and pressure to 25-26 mmHg, and then shot. Cell were allowed to recover in 2% PPY media (0.02 g/mL protease peptone, 0.002 g/mL yeast extract) for seven hours at 30°C, and subsequently plated in 96-well plates. Cells were selected with 20 µM Paclitaxel (Fisher Scientific). After three to seven days, surviving *Tetrahymena* were placed in 24-well plates with 40 µM Paclitaxel.

Knock Down Confirmation via Whole-Cell PCR

Both CU428 and shRNA-RAD4 *Tetrahymena thermophila* strains were grown in

24-well plates and treated with 20 μM Paclitaxel for 2-3 days. PCR reactions were made by adding 3 μL of growing cells to 1X GoTaq MasterMix (Promega), 10 pmol shRNA forward and reverse confirmation primers to a final reaction volume of 25 μL. A similar reaction was performed for the positive control but in place of the growing cells a 1:200 dilution of the linearized shRNA-RAD4 plasmid was used. Samples were heated to 95°C for 2 minutes and then cycled through amplification 32 times at 95°C for 45 seconds, 60.6°C for 45 second, and 72°C for 1 minute 45 seconds. The samples are left at 72°C for 5 minutes, and the temperature was lowered to 4°C (MJ Mini Personal Thermocycler, Bio Rad). Products were run on a 1.5% agarose gel in TAE at 120V for 30 minutes and visualized with the KODAK Gel Logic 200 Imaging System.

Total RNA Isolations

Tetrahymena thermophila cultures (CU428 and shRNA-RAD4 knock down strains) were grown to $1x10^5$cell/mL. Cells were centrifuged for 3 minutes at 3000 rpm (Sorvall Legend X1 Centrifuge, Thermo Fisher Scientific), and washed with 10 mM Tris. Cells that necessitated UV treatment were resuspended in 10 mL of 10 mM Tris and treated with 100 J/m^2 UV, and were allowed to recover for two hours. Total RNA was isolated with the Qaigen RNeasy mini kit according to the manufacturers recommendations. Briefly, cells were thoroughly resuspended in 600 μL RLT Buffer with 143 mM β-mercaptoethanol. One thousand μL 70% Ethanol was added and the solution was transferred to RNeasy spin column. Column was centrifuged at maximum speed for 15 seconds. The flow through was discarded, and 350 μL Buffer RW1 and centrifuged at maximum speed for 15 seconds. Then 80 μL of RDD solution with 30 U

RNase-free DNase I (Qiagen). This sample was incubated on the column at room temperature for 15 minutes, and 350 µL Buffer RW1 was added and centrifuge at maximum speed for 15 seconds. Then 500 µL of Buffer RPE was added and centrifuged at maximum speed for 15 seconds. Flow through was discarded and 500 µL of Buffer RPE was added and centrifuged at maximum speed for 2 minutes. The column is transferred to a new collection tube and 50 µL of RNase free water (Qiagen). RNA samples were quantified (NanoDrop 2000 Spectrophotometer, Thermo Fisher Scientific), and samples were stored at -80°C.

Quantitative Reverse Transcriptase Polymerase Chain Reaction (qRT-PCR)

cDNA was created by combining 1X AMV Buffer (Promega), 5 mM M_gCl_2, 2 µL 10 mM dNTPs (Promega), 1 µL RNasin-RNase Inhibitor (Thermo Fisher Scientific), 7.5 units AMV Reverse Transcriptase (Promega), and 5 µM Oligo dTVN (IDT), and then 2 µg of Total RNA isolation was added to aliquoted master mix and incubated at 42°C for 25 minutes, 99°C for 5 minutes, and 4°C for 5 minutes.

Quantitate Reverse Transcriptase polymerase chain reactions were created by adding 1X SsoFast EvaGreen (Bio Rad), 10 µM of forward and reverse primer (qRT-PCR RAD4, shRNA Confirmation, HHP1 or ACT1; Table 1) were added to 1 µL cDNA, water or gDNA. These samples were placed in the Bio Rad CFX Connect Real-Time Detection System. They were heated to 95°C for 2 minutes and then the following three steps 32 times: 95°C for 45 seconds, 54°C for 45 second, and 72°C for 1 minute 45 seconds. The samples are left at 72°C for 5 minutes, and allowed to heat to their full melting temperatures. The Bio Rad CFX Connect Real-Time Detection Software

determines the Starting Quantities (SQ) of qRT-PCR products on the basis of the gDNA dilutions with the ACT1 primers. The samples were then normalized to the HHP1 expression levels for the respective treatments, and made relative to either no treatment or wild type cells.

Survivability Assay of *Rad4* Knock Down Strains in *T. thermophila*

Tetrahymena thermophila cultures (CU428 and shRNARAD4 knock down strains) were grown to $1x10^5$cells/mL, and the treated with various levels of UVC treatment (0, 25, 50, 75, and 100 J/m^2). Treatment occurred in 10 mM Tris in the CL-1000 Ultraviolet Crosslinker, UVP, and one mL of treated cells was added to 9 mL 10 mM Tris, and vortexed. This process was repeated, and 0.6 mL of this dilution was added to 29.4 mL 2% PPY+1XPSF. Cells were plated in 96-well plates and incubated in humidity chambers at 30°C for 7 days. After 7 days, wells with significant growth were counted. No UV treatment (0 J/m^2) was considered 100% survivability.

***T. thermophila* Genomic DNA Isolation**

Tetrahymena thermophila cultures (CU428 and shRNA-RAD4 knock down strains) were grown to $1x10^5$cells/mL. Cells were centrifuged for 3 minutes at 3000 rpm (Sorvall Legend X1 Centrifuge, Thermo Fisher Scientific), and were washed with 10 mM Tris. Samples treated with UV in the CL-1000 Ultraviolet Crosslinker, UVP with 100 J/m^2 UVC. Samples were isolated from untreated, 0, 1, 2, 3, and 4 hours after UV treatment. After samples are centrifuge for 3 minutes at 3000 rpm (Sorvall Legend X1 Centrifuge, Thermo Fisher Scientific). The pellet was washed with 10 mM Tris then

lysed with 3.5 mL Urea Lysis Buffer. 700 µL of the lysate was aliquoted to 1.5 mL microcentrifuge tubes and DNA was phenol chloroform extracted twice. Aqueous samples were frozen overnight at -20°C. Samples were thawed and 0.88 M NaCl, and equal volumes of isopropanol were added. Samples were centrifuged (Spectrafuge 24D Digital Microcentrifuge) at maximum speed for 10 minutes. Supernatant was decanted and 500 µL of the pellet was washed with 70% ethanol at room temperature for two minutes. Samples were centrifuged for three minutes at maximum speed, the supernatant decanted and the DNA pellet was dried. Fifty µL of Tris-EDTA (100 mM Tris-HCl, 10 mM EDTA) buffer was added to each DNA pellet, and all samples containing the same treatment and strain are combined. Genomic DNA (gDNA) samples were incubated with 10 mg/mL RNase A (AppliChem Panreac) at 37°C for 3 hours. Samples were quantified with a NanoDrop spectrometer (NanoDrop 2000 Spectrophotometer, Thermo Fisher Scientific).

DIG-Labeled Telomere Probe Detection Assay

gDNA (5 µg) were digested overnight at 37°C with HindIII-HF (NEB) in 1X SmartCut Buffer. Digests were electrophoresed on a 1.5% agarose gel for 3 hours (or until migrated three-fourths down the gel for maximum separation) at 70V, then stained with 10 mg/mL ethidium bromide for 5 to 10 minutes, and visualized with the KODAK Gel Logic 200 Imaging System. Any gel not containing sample is removed, and gel is destained for 15 minutes in water and then depurinated in 0.125 N HCl for 20 minutes, and rinsed with water. Gel was washed in denaturing solution (1.5 M NaCl, 0.5 NaOH) for 20 minutes, and rinsed with water. Gel was washed in neutralizing solution (1.5 M

NaCl, 0.5 M Tris base) for 20 minutes, and rinsed. The agarose gel was placed in a Pyrex dish with 10X SSC (3.0 M NaCl, 0.3 M Sodium Citrate, pH adjusted to 7.0 with 1 N HCl) on top of the wick (made from stacked chromatography paper, Whatman and paper towels), then topped with a piece of prewet nitrocellulose membrane (Whatman Nytran SuPerCharge Membrane), two pieces of chromatography paper, 3 inches of paper towels, and a glass weight. This transfer apparatus was left overnight for approximately 12 hours. The next day, the nitrocellulose membrane was UV cross linked (CL-1000 Ultraviolet Crosslinker, UVP) at 1200 J/m^2 twice, and stored at 4°C.

All incubation of the nitrocellulose membrane occurred in a rotating hybridization oven at the specified temperature. The membrane was washed in 0.1X SSC/0.1% SDS for one hour at 65°C. Membrane was prehybridized with 10X Denhardt's Solution, (ThermoFisher Scientific), 6X SSC, 0.1% SDS for an hour at 40°C. The Digoxygenin (DIG)-Telomere and Digoxygenin (DIG)-ACT1 telomere probes (Table 1) at 100 µM was added and allowed to hybridize for approximately 12 to 15 hours. The hybridization solution was removes and the membrane was washed with three times with 6X SSC/0.1%SDS at 42°C for two minutes, ten minutes, and another ten minutes. The membrane was washed at 45°C in 6X SSC/0.1%SDS for twenty minutes.

The membrane was blocked in 0.5% milk in TBST with 0.002% Tween 20 (Biorad) for one hour, and then incubated for 1.5 hours in TBST with 1:1000 anti-Dig antibody (Anti-Dig-POD, Fab fragments Roche). The membrane was washed in new TBST for five minutes, 15 minutes, and another 15 minutes, and finally for 15 minutes in TBS. To visualize the restriction fragment lengths, the membrane was covered in a one to one ratio of SuperSignal West Dura Stable Peroxide Buffer and SuperSignal West Dura

Lumino/Enhancer Solution (Thermo Scientific). The membrane was visualized using both the LI-COR Odyssey FC (5 and 15 minutes exposures) and the Agfa CP1000 Automatic Film Processor (10 seconds, 30 seconds, 1 minute, 5 minutes, and 30 minutes exposure).

Statistical Analysis

For statistical analysis of the qRT-PCR data, a One-Way ANOVA was performed with IMB SPSS 20.0. To test the differences between untreated expression levels and 0, 1, 2, 3, and 4 hours after treatment a Tukey's HSDs were calculated. Error bars were calculated by plotting plus or minus the standard error of the mean.

For statistical analysis of the survivability assays, a One-Way ANOVA was performed with IMB SPSS 20.0. To test the difference between no treatment and the various condition types and between the same treatments a Tukey's HSDs was conducted. Error bars were calculated by plotting plus or minus the standard error of the mean. The effect size was calculated with a t-test assuming equal variances with the equation $(t^2-1)/(t^2+df+1)$.

For statistical analysis of the knock down confirmation qRT-PCR, a One-way ANOVA was performed with IMB SPSS 20.0. To test the difference between wild type and knock down strains treated and untreated a Tukey's HSDs was conducted.

RESULTS

Conservation of Shelterin and XPC/RAD4 Proteins

Shelterin proteins from *Tetrahymena thermophila, Homo sapiens, Saccharomyces cerevisiae, and Schizosaccharomyces pombe* were analyzed for the presence of predicted domains and sites using InterPro (Table 3). Upon analysis many of the shelterin protein sequences did not contain any identifiable domains (data not shown). The most conserved domains amongst the shelterin proteins were found in the POT1 proteins and POT1 associated proteins. Outside of those domains there was large divergence in type and position of domains in these proteins between model organisms. Even though many of the functions are conserved, it is sometimes difficult to find homologs based on amino acid sequence in other organisms.

Rad4 (TTHERM_00825460) amino acid sequence in *T. thermophila* was analyzed with BLAST to find homologous amino acid sequences in frequently studied model organisms. There was a conservation in domain type and position in all the model organisms studied (see Bioinformatics in Experimental Procedures). Because of this quality, any research conclusions of *RAD4* in *Tetrahymena thermophila* can be more readily applied across organisms rather than shelterin, which diverges significantly. Ras4 (XPC) homologs were acquired from *Homo sapiens, Mus musculus, Danio rerio, Xenopus laevis, Caenorhabditis elegans, Drosophila melanogaster, Dictyostelium discoideum, Saccharomyces cerevisiae, Schizosaccharomyces pombe, Zea mays, Arabidopsis thaliana, Vitis vinifera,* and *Aspergillus niger* (Table 4). All identified homologs contain four characteristic domains of Rad4 proteins: transglutaminase-like

Table 3. Shelterin Proteins InterPro Domain Analysis

Species	Gene	Diagram[1]	Size (aa)	Domain Locations[1]
Tetrahymena thermophila	POT1	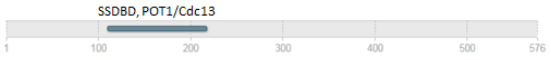	576	SSDBD,POT1/ Cdc13: 111-218
Tetrahymena thermophila	TPT1		992	EFH: 34-105, 157-192, 193-228, 794-865, 919-990
Homo sapiens	POT1	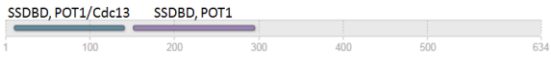	634	SSDBD,POT1/ Cdc13: 11-141 SSDBD,POT1: 152-296
Homo sapiens	TRF1		439	TRBF,Dim: 77-269 Myb: 375-432
Homo sapiens	TRF2	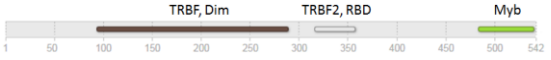	542	TRBF,Dim: 77-269 TRBF2,RBD: 317-358 Myb: 484-541
Homo sapiens	RAP1		399	BRCT: 18-100 Myb: 132-195 TRF2/RBD 322-397
Homo sapiens	TIN2	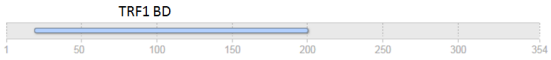	354	TRF1 BD: 20-201
Saccharomyces cerevisiae	CDC13	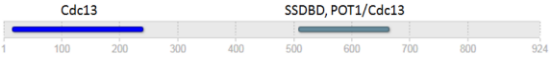	924	Cdc13: 16-241 SSDBD,POT1/ Cdc13: 448-579
Saccharomyces cerevisiae	RAP1	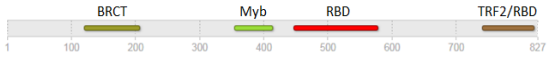	827	BRCT: 121-208 Myb: 355-415 RBD: 490-543 TRF2/RBD: 551-626
Saccharomyces cerevisiae	RIF1	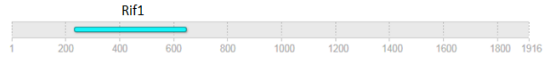	1916	Rif1: 234-649
Schizosaccharomyces pombe	CCQ1	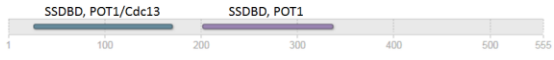	555	SSDBD,POT1/ Cdc13: 27-171 SSDBD,POT1: 203-338
Schizosaccharomyces pombe	RAP1		693	BRCT: 81-105 DBD: 495-602
Schizosaccharomyces pombe	TRF1		663	TRBF,Dim: 125-351 RBD: 452-496 Myb: 557-612

[1]SSDBD,POT1/Cdc13: single stranded DNA binding domain, POT1/Cdc13; EFH: EF-Hand; TRBF, Dim: Telomere Repeat Binding Factor, Dimerization; RBD: Rap1 Binding Domain; BRCT: BRCA1 C Terminus; DBD: DNA binding domain

Table 4. XPC/Rad4 InterPro Domain Analysis

Species[1]	Gene	Diagram[2]	Size (aa)	Domain Locations[2]
Tetrahymena thermophila	RAD4		934	TGF: 542-622 βHD1: 707-759 βHD2: 707-759 βHD3:815-889
Homo sapiens	XPC	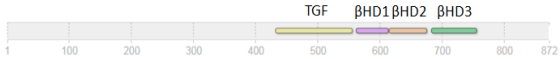	872	TGF: 433-557 βHD1: 562-614 βHD2: 616-676 βHD3:683-757
Mus musculus	XPC	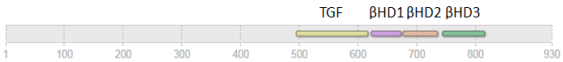	930	TGF: 495-618 βHD1: 623-675 βHD2: 677-737 βHD3:744-818
Danio rerio	XPC	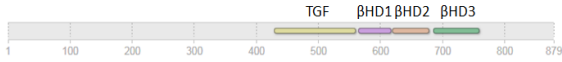	879	TGF: 430-561 βHD1: 566-618 βHD2: 620-679 βHD3: 686-760
Xenopus laevis	XPC	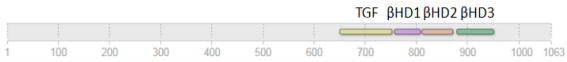	1063	TGF: 651-753 βHD1: 758-810 βHD2: 812-872 βHD3: 879-953
Caenorhabditis elegans	XPC	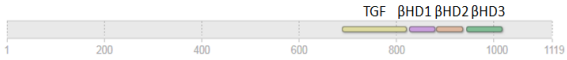	1119	TGF: 689-822 βHD1: 827-881 βHD2: 883-938 βHD3: 945-1091
Drosophila melanogaster	XPC		1293	TGF: 689-822 βHD1: 827-881 βHD2: 883-938 βHD3: 945-1091
Dictyostelium discoideum	RAD4	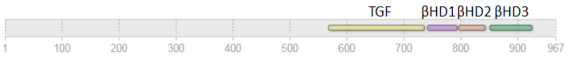	967	TGF: 689-822 βHD1: 827-881 βHD2: 883-938 βHD3: 945-1091
Saccharomyces cerevisiae	RAD4	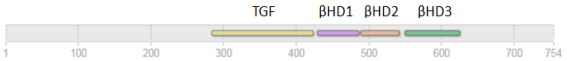	754	TGF: 285-425 βHD1: 430-488 βHD2: 490-543 βHD3: 551-626
Schizosaccharomyces pombe	RHP42	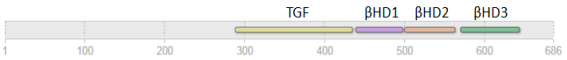	686	TGF: 289-436 βHD1: 440-499 βHD2: 501-564 βHD3: 571-645
Zea mays	RAD4	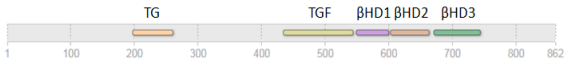	862	TG: 198-262 TGF: 435-545 βHD1: 550-601 βHD2: 603-665 βHD3: 672-746
Arabidopsis thailana	RAD4	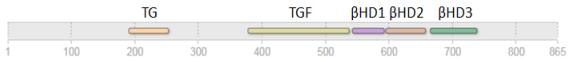	865	TG: 191-254 TGF: 379-538 βHD1: 543-594 βHD2: 596-659 βHD3: 666-740
Vitis vinifera	RAD4	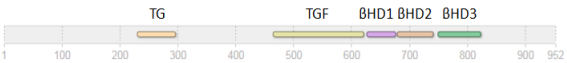	952	TG: 231-297 TGF: 466-622 βHD1: 627-678 βHD2: 680-743 βHD3: 750-824
Aspergillus niger	RAD4	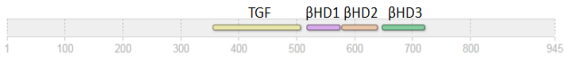	945	TGF: 356-508 βHD1: 519-576 βHD2: 578-641 βHD3: 648-722

[1]Blue: protozoa, Red: metazoa, Green: helminth, Purple: fungi, Yellow: plants
[2]TGF: transglutaminase-like fold, β-Hairpin Domain 1-3, TG: Transglutaminase

fold (TGF), Beta-hairpin loop 1 (βHD1), βHD2, and βHD 3 (Table 4). An additional transglutaminase domain was present near the N-terminus in the three plant species analyzed (*Zea mays, Arabidopsis thaliana,* and *Vitis vinifera).*

To further analyze the evolutionary conservation of Rad4 homologs and reinforce the validity of *Tetrahymena thermophila* as a effective model organism for studying *RAD4*, these same protein sequences were organized by phylogeny with MEGA 7.0 (Figure 5). There are two large initial diverges that occurred in evolution: one clade contains metazoa, plants, helminth, and protozoa, and the other clade contains fungi. The metazoa (*H. sapiens, M. musculus, X. laevis, D. rerio*, and *D. melanogaster*) grouped together. The only helminth, *C. elegans*, grouped alone. The two protozoa *D. discoideum* and *T. thermophila* diverged together off of the first clade. The three fungi in the other clade contained *A. niger, S. pombe,* and *S. cerevisiae.* Because the *T. thermophila* is diverging in the first clade with metazoa, plants, and helminth, its sequence is more evolutionarily conserved than the sequence of the fungi Rad4 proteins.

Quantification of *Tetrahymena thermophila RAD4* Expression Levels Before and After Damage

To more completely understand the role of *RAD4* in DNA repair, *RAD4* expression levels were measured by qRT-PCR after three different genotoxic stressors that lead to different type of DNA damage, repaired by different mechanisms: UV light causes pyrimidine dimers that are repaired by nucleotide excision repair. Hydrogen peroxide treatment causes oxidation of the nucleotide bases and hydrolysis of the phosphodiester that is repaired by base excision repair. Methyl methanesulfonate (MMS)

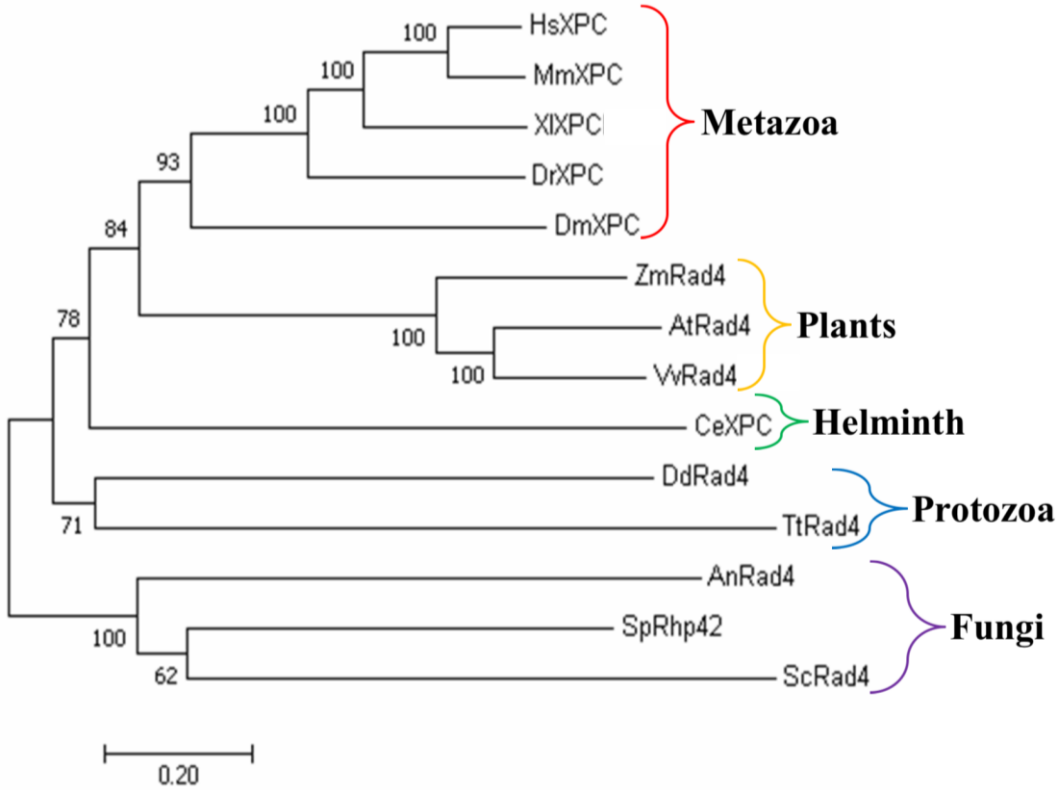

Figure 5. Maximum Likelihood Phylogenetic Tree of XPC/Rad4. The domains of commonly studied model organisms were analyzed against Rad4 amino acid sequence in *Tetrahymena thermophila*. This evolutionary comparison was inferred through the maximum likelihood method with a bootstrap consensus taken from 1000 replicates using MEGA 7.0. The model organism's abbreviations are T.t. *Tetrahymena thermophila,* H.s. *Homo sapiens,* M.m. *Mus musculus,* D.d *Danio rerio,* X.l. *Xenopus laevis,* C.e. *Caenorhabditis elegans,* D.r. *Drosophila melanogaster,* D.d *Dictyostelium discoideum,* S.c. *Saccharomyces cerevisiae,* S.p. *Schizosaccharomyces pombe,* Z.m. *Zea mays,* A.t. *Arabidopsis thaliana,* V.v. *Vitis vinifera,* and A.n. *Aspergillus niger.*

adds methyl groups to DNA strands that ultimately leads to double stranded breaks repaired by homologous recombination or nonhomologous end joining (Weeden and Asselin-Labat, 2018).

To analyze the qRT-PCR data, an amplification curve, melt peak, and agarose gel visualizing a set of the qRT-PCR *RAD4* (Figure 6A, 7A, 8A) and *HHP1* (H1/HP1-like; Figure 6C, 7C, and 8C) products. The analysis of *HHP1* was included as a housekeeping gene which maintains expression levels before and after genotoxic stressors. This allowed for later data normalization. An amplification curve measures the relative florescent units (RFU) during each cycle of amplification. In all treatments the amplification curves show a variety of *RAD4* expression levels. *HHP1* showed relatively consistent amount of amplification amongst treatments. Additionally, in these curves, actin amplification curves are included (colored in red). This creates a standard curve using 1000 ng, 100 ng, 10 ng, and 1 ng of genomic DNA with actin primers.

Melt peaks were analyzed for both the *RAD4* and *HHP1* as indicator of a singular product. One peak indicates that a single product is in the reaction that is melting or dissociating at a specific temperature. The melt peaks showed specific peaks representing *RAD4* (Figure 6B, 7B, and 8B) and *HHP1* (Figure 6D, 7D, and 8D) in one peak and *ACT1* control in the other, indicating that there was specific amplification of the appropriate products during qRT-PCR.

The products of both *RAD4* and *HHP1* were also separated by agarose gel electrophoresis. A single band at the expected length with *RAD4* (186 base pairs) and *HHP1* (216 base pairs) was observed on the gel (Figure 6E,7E, 8E), further suggesting specific amplification of *RAD4* and *HHP1* products by qRT-PCR. Also, both the *RAD4*

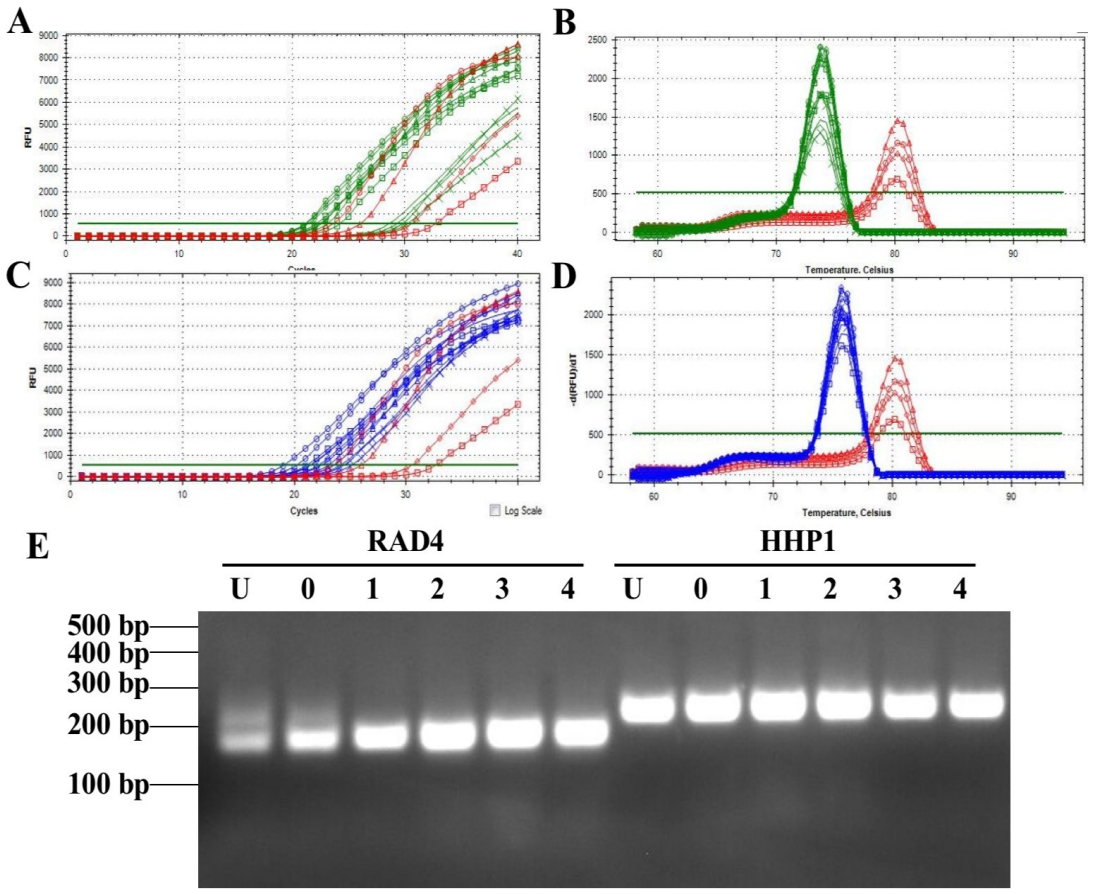

Figure 6. Quantification of *RAD4* Expression After Ultraviolet (UV) Treatment. (A) Amplification curve of the amount of *RAD4* (green) and *ACT1* (red) during each cycle of qRT-PCR amplification. (B) Melt peak of qRT-PCR products with primers to *RAD4* (green) and *ACT1* (red). (C) Amplification curve of *HHP1* control (blue) and *ACT1* (red). (D) Melt peak of qRT-PCR products with *HHP1* (blue) and *ACT1* (red). In both the *RAD4* and *HHP1* amplification curves and melt peaks show no treatment (U; line), 0 hours after treatment (0; cross), 1 hour after treatment (1; circle), 2 hours after treatment (2; triangle), 3 hours after treatment (3; diamond), and 4 hours after treatment (4; square). *ACT1* standards (red) were used to establish a standard curve with 1000 ng genomic DNA (circle), 100 ng genomic DNA (triangle), 10 ng genomic DNA (diamond), and 1 ng genomic DNA (square). (E) Agarose gel (1.5% in TAE) of a representative set of *RAD4* and *HHP1* products as a result of qRT-PCR.

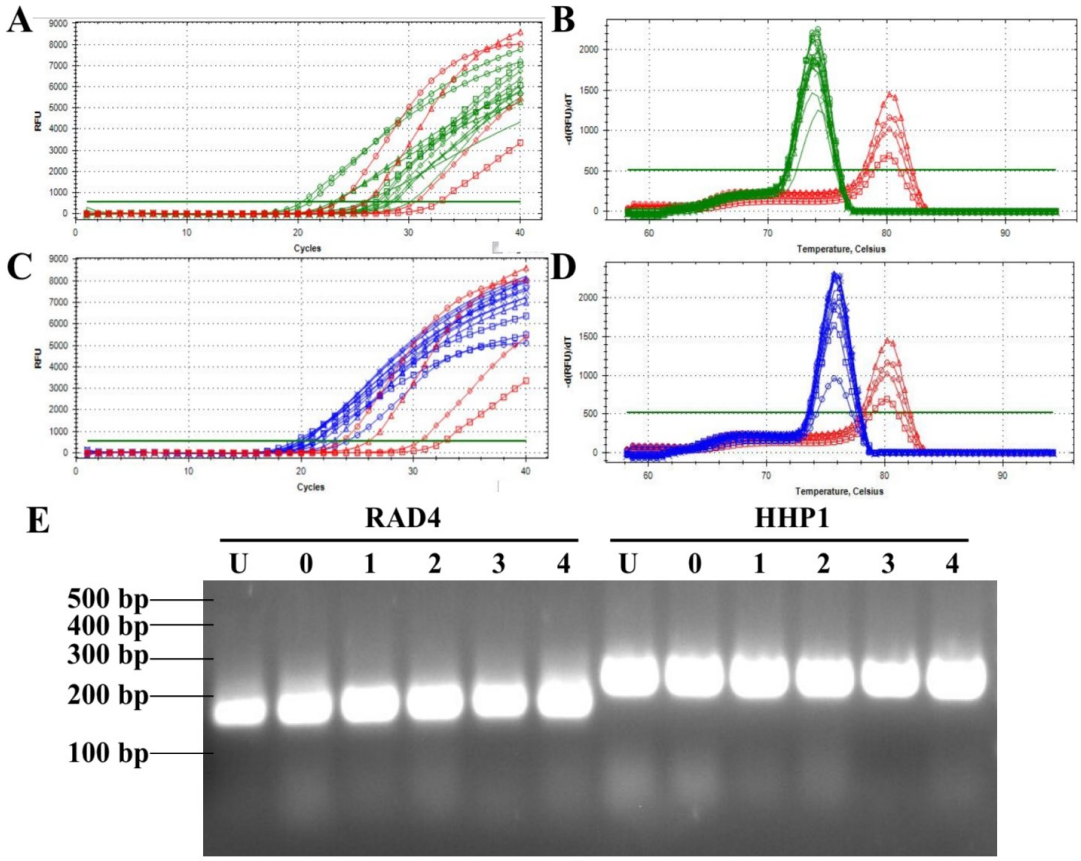

Figure 7. Quantification of *RAD4 E*xpression After Hydrogen Peroxide (H_2O_2) Treatment. (A) Amplification curve of the amount of *RAD4* (green) and *ACT1* (red) during each cycle of qRT-PCR amplification. (B) Melt peak of qRT-PCR products with primers to *RAD4* (green) and *ACT1* (red). (C) Amplification curve of *HHP1* control (blue) and *ACT1* (red). (D) Melt peak of qRT-PCR products with *HHP1* (blue) and *ACT1* (red). In both the *RAD4* and *HHP1* amplification curves and melt peaks show no treatment (U; line), 0 hours after treatment (0; cross), 1 hour after treatment (1; circle), 2 hours after treatment (2; triangle), 3 hours after treatment (3; diamond), and 4 hours after treatment (4; square). *ACT1* standards (red) were used to establish a standard curve with 1000 ng genomic DNA (circle), 100 ng genomic DNA (triangle), 10 ng genomic DNA (diamond), and 1 ng genomic DNA (square). (E) Agarose gel (1.5% in TAE) of a representative set of *RAD4* and *HHP1* products as a result of qRT-PCR.

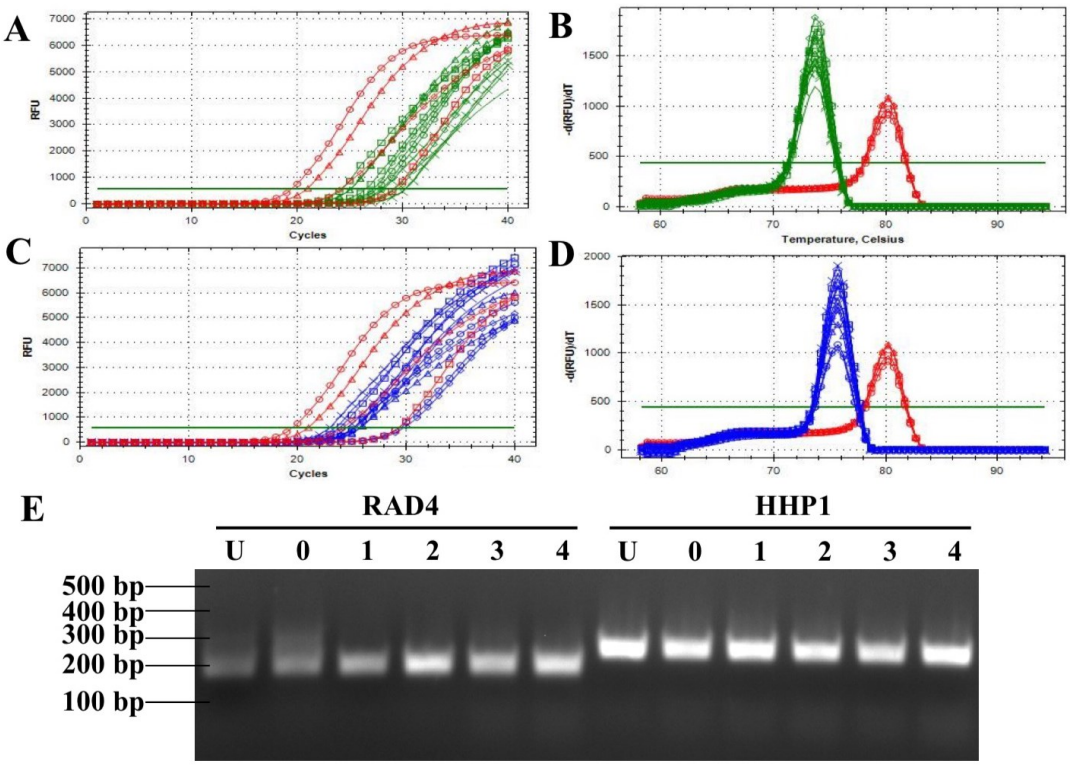

Figure 8. Quantification of *RAD4* Expression After Methyl Methanesulfonate (MMS) Treatment. (A) Amplification curve of the amount of *RAD4* (green) and *ACT1* (red) during each cycle of qRT-PCR amplification. (B) Melt peak of qRT-PCR products with primers to *RAD4* (green) and *ACT1* (red). (C) Amplification curve of *HHP1* control (blue) and *ACT1* (red). (D) Melt peak of qRT-PCR products with *HHP1* (blue) and *ACT1* (red). In both the *RAD4* and *HHP1* amplification curves and melt peaks show no treatment (U; line), 0 hours after treatment (0; cross), 1 hour after treatment (1; circle), 2 hours after treatment (2; triangle), 3 hours after treatment (3; diamond), and 4 hours after treatment (4; square). *ACT1* standards (red) were used to establish a standard curve with 1000 ng genomic DNA (circle), 100 ng genomic DNA (triangle), 10 ng genomic DNA (diamond), and 1 ng genomic DNA (square). (E) Agarose gel (1.5% in TAE) of a representative set of *RAD4* and *HHP1* products as a result of qRT-PCR.

an *HHP1* qRT-PCR primers spanned introns, so a band of significantly larger size would have been present if genomic DNA was contaminating the RNA sample.

The *RAD4* expression levels were quantified and normalized to *HHP1*. *RAD4* expression increased 129-, 161-, and 93-fold following two, three, and four hours after a 100 J/m^2 UV, respectively (Figure 9A). These changes indicate that *RAD4* expression was induced by DNA damage, consistent with proteins involved in nucleotide excision repair (Figure 9A and 9D). After a one hour period of hydrogen peroxide treatment there is a significant increase *RAD4* expression (108-fold) at one hour with a gradual decrease after this peek (Figure 9B and 9D). This pattern of expression implicates *RAD4* in DNA repair. MMS treatment yields one increase in *RAD4* expression, but the other increases cycle up and down. It is likely that there was no involvement of *RAD4* in double stranded break repair (Figure 9C and 9D). Overall, we conclude that *RAD4* plays a prominent role in nucleotide excision repair and base excision repair.

Established *Rad4* Knock Down Strains in *T. thermophila*

To further understand the role of *RAD4*, strains of *T. thermophila* where *Rad4* expression was depleted were established. A plasmid was designed that will knock down expression of *Rad4* by RNA interference (pBT1-shRNA:RAD4). Primers that contained the sense and antisense strands of a short-hairpin RNA (shRNA) gene were incorporated into pBT1-shRNA:RAD4 (Figure 10A, represented in red). When transcribed, the sense and antisense strands formed a stem loop structure which has a ΔG of -24.45 kcal·mole^{-1} (Figure 10B). The plasmid contains a beta-tubulin recombination site that will serve as recombination arms at the native beta-tubulin 1 (*BTU1*) site during biolistic

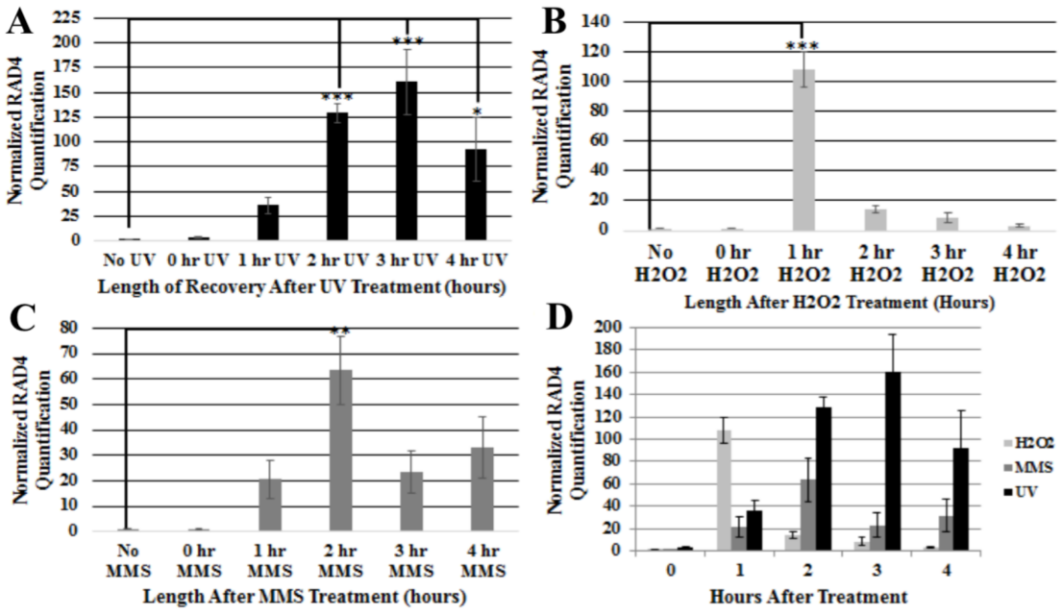

Figure 9. *RAD4* Expression Quantification After Hydrogen Peroxide, Methyl Methanesulfonate, and Ultraviolet Light Treatment. *RAD4* expression was measured via quantitative reverse transcriptase PCR following exposure to (A) 100 J/m^2 UV light, (B) 0.5 mM H_2O_2, and (C) 5.0 mM MMS. Expression was normalized to *HHP1*. Error bars represent +/- standard error of mean. *p value <0.05, **p value <0.01, ***p value <0.005 which were determined by a One-Way ANOVA with Tukey's HSDs. (D) Data were combined and set relative to no treatment. n≥3.

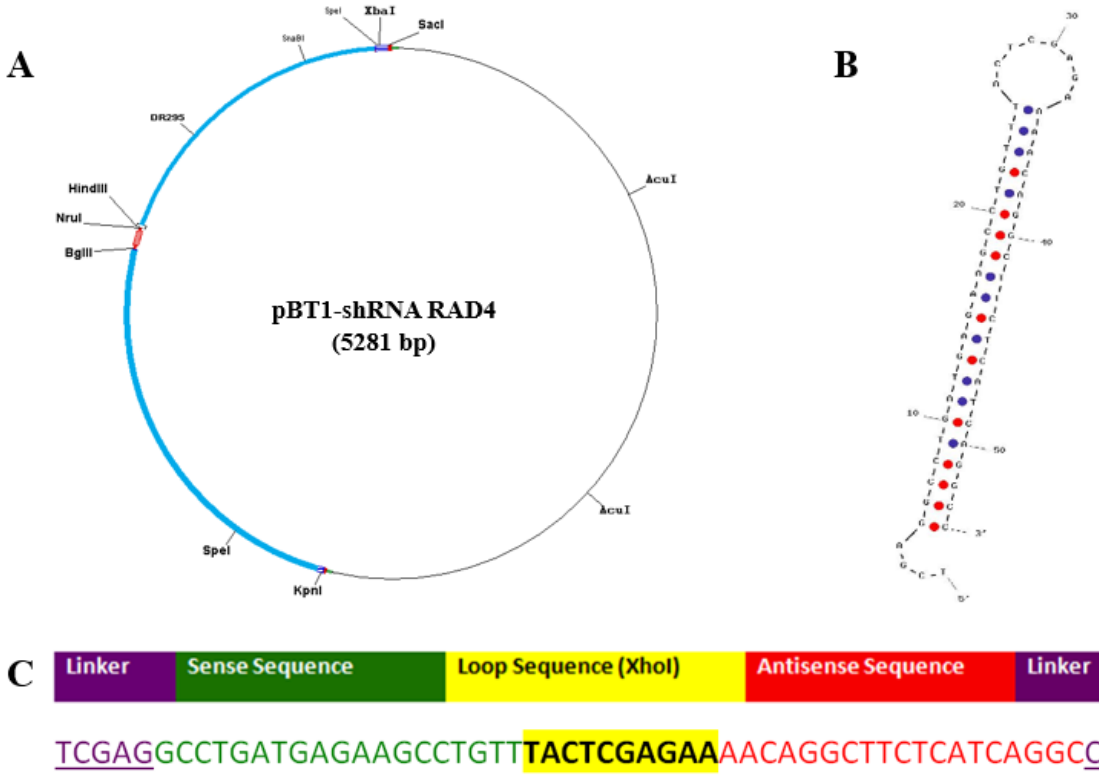

Figure 10. Construction of pBT1-shRNA:RAD4. (A) pBT1-shRNA:RAD4 plasmid map containing a red segment with *RAD4* sense and antisense primers, light blue segment in the beta-tubulin 1 (*BTU1*) recombination site, and various restriction enzyme sites. (B) Stem-loop representation of the *Rad4* hairpin structure (21 nucleotides). The ΔG is -24.45 kcal·mole^{-1}. (C) Sequence and diagram representation of stem-loop sequence. Purple represents the linker region. Green represents the *Rad4* sense sequence and red represents the *Rad4* antisense sequence. Yellow represents the loop portion and *XhoI* restriction enzyme site.

transformation into *T. thermophila.* (Figure 10A, represented in light blue). When transformed into DH10B cells, pBT1-shRNA:RAD4 produced 1 CFU with 10 ng of plasmid, and 14 CFUs with 50 ng of plasmid. Negative controls were analyzed; pBT1-YFG with no insert and no ligase produced 2 CFUs with 10 ng of plasmid, and 9 CFUs with 50 ng of plasmid.

DNA was isolated from DH10B containing pBT1-shRNA:RAD4 and cloning was confirmed by restriction digest. The shRNA insertion has a unique *XhoI* cut site (Figure 10C), therefore, digestion with *XhoI*, and a restriction enzyme that uniquely cuts within the backbone (*Sac*I) will produce unique fragments. The predicted products of the *Xho*I/*Sac*I digest are 1070 and 4214 base pairs. Only one clone contained the expected products (Figure 11, clone 4), and was selected for further use. The shRNA plasmid DNA was linearized with *KpnI* and *SacI* (data not shown). This linearized product was then transformed and selected in *T. thermophila* via paclitaxel. Whole-cell PCR was performed to confirm the presence of pBT1-shRNA:RAD4 (Figure 12). Samples not transformed were expected to amplify only the *BTU1* (native) locus (1750 bp), while cells that successfully incorporated the *Rad4* shRNA knock down will amplify a 500 bp region containing the shRNA insert. Products corresponding to amplification of the shRNA were most intensely amplified in the digested plasmid (positive control), and CU522 clone 1 and 10 and CU725 clone 11. These clones were selected as *Rad4* knockdowns subjected to further analysis.

Verification of *Rad4* Knock Down in *T. thermophila*

To verify that expression of *RAD4* is affected by introduction of the *Rad4* shRNA,

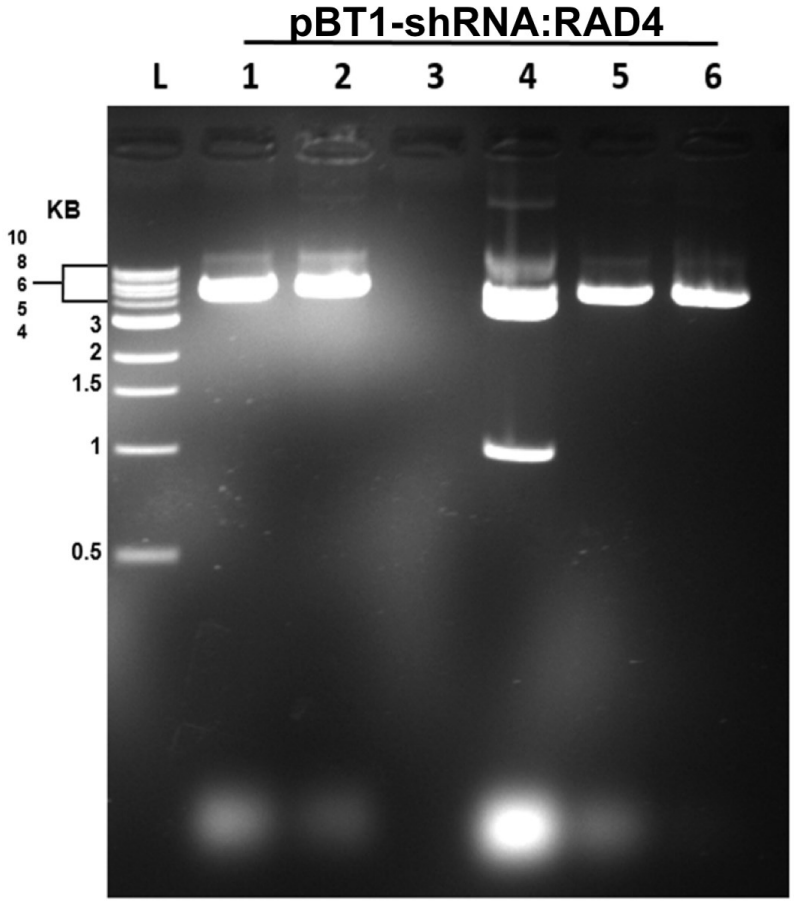

Figure 11. Digest of pBT1-shRNA:RAD4. Agarose gel (1.5% in TAE) of purified plasmid DNA digested with *XhoI* and *SacI*. Lane L has a 1 kilobase ladder with sizes indicated to the left (KB). Lanes marked 1 to 6 contain clones from pBT1-shRNA:RAD4 cloning attempt. The expected band sizes for pBT1-shRNA:RAD4 are 4214 and 1070 base pairs.

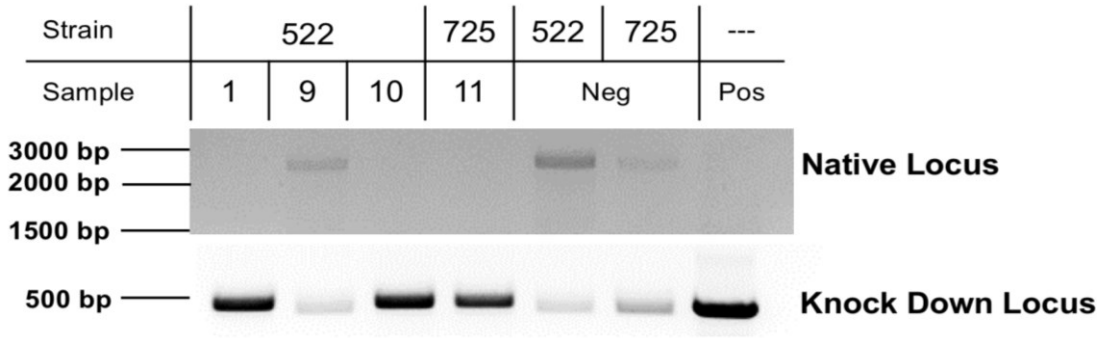

Figure 12. Knock Down Confirmation via Whole-Cell PCR. Whole-cell PCR was conducted on four possible *T. thermophila* transformants with pBT1-shRNA:RAD4. The primers amplify either the native Beta-tubulin 1 locus creating an approximate 1750 base pair product (top). The primers should amplify a 500 base pair product in strains containing the shRNA (bottom). The negative control lanes (Neg) contain untransformed cells. The positive control (Pos) contains undigested pBT1-shRNA:RAD4 and will amplify only the shRNA.

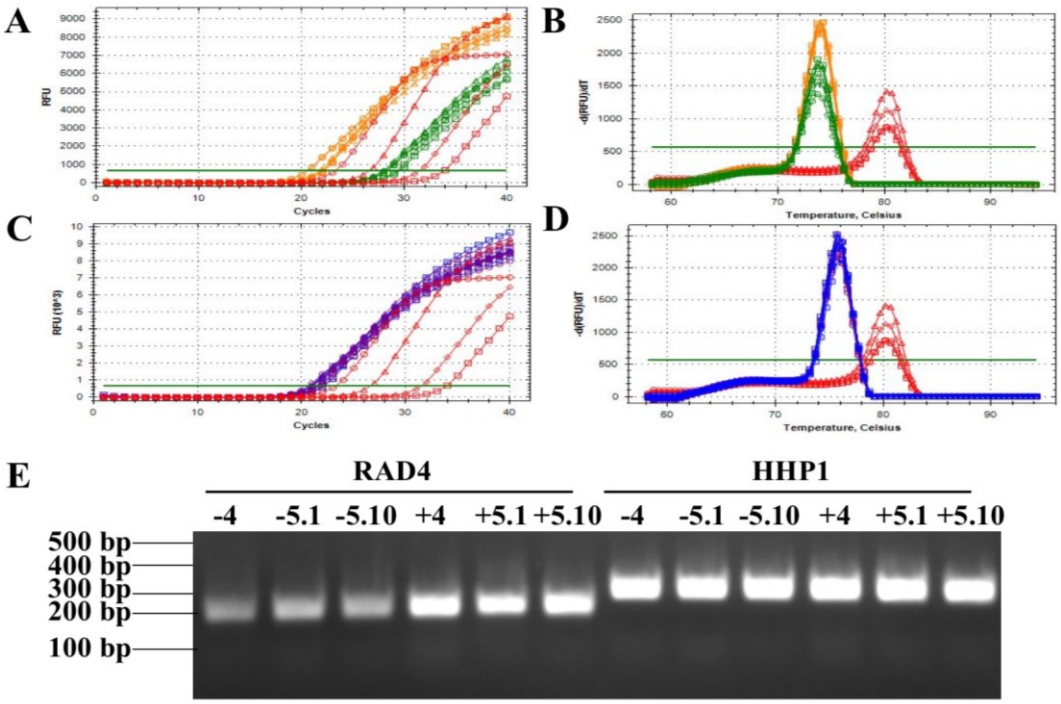

Figure 13. Quantification of *RAD4* Expression in the *Rad4* Knock Down Strains. (A) Amplification curve of *RAD4* during each cycle of qRT-PCR amplification. (B) Melt peak of qRT-PCR products with primers to *RAD4* and *ACT1*. Samples were treated with UV (orange), and untreated (green). (C) Amplification curve of *HHP1* control. (D) Melt peak of qRT-PCR products with primers to *HHP1* and *ACT1*. Samples were treated with UV (blue), and untreated (purple). Wild type (circle), *Rad4* knock down clone 1 (triangle), *Rad4* knock down clone 10 (Square). *ACT1* standards (red) were used to establish a standard curve with 1000 ng genomic DNA (circle), 100 ng genomic DNA (triangle), 10 ng genomic DNA (diamond), and 1 ng genomic DNA (square). (E) Agarose gel (1.5% in TAE) of a representative set of *RAD4* and *HHP1* qRT-PCR products. WT (4), knock down clone 1 (5.1) and knockdown clone 10 (5.10) were either untreated (-), or treated with 100 J/m^2 UV treatment and were allowed to recover for two hours after treatment (+).

qRT-PCR was performed on wild type and RAD4 knock down clones 1 and 10. Based on phenotypic results, qRT-PCR analysis was not performed on CU725 clone 11. In all treatments the amplification curves showed a variety of *RAD4* expression levels. (Figure 13A). The *HHP1* house keeping genes showed tightly grouped amplification regardless of the treatment, (blue: UV, purple: no UV) as expected (Figure 13C). Actin 1 was amplified from defined amounts of genomic DNA to provide a standard curve for detection (Figure 13, red). Isolated melt peaks appear for *RAD4*, *HHP1,* and *ACT1*, indicating specific products for each (Figure 13B and 13D). Furthermore, electrophoresis of the qRT-PCR products of both *RAD4* and *HHP1* showed a single amplicon at the appropriate size for each product (186 and 278 bp, respectively; Figure 13E). Both the specific melt peak, and the singular amplicon on the agarose gel suggest specific amplification of *RAD4* and *HHP1* products by qRT-PCR.

RAD4 expression levels in the knock down strains were quantified, and normalized to *HHP1* (Figure 14). *Rad4* knock down clone 1 showed 50% reduction in expression after UV exposure ($p = 0.001$), when compared to wild type, indicating successful knockdown of *RAD4* expression by the shRNA. This difference in expression was seen more drastically following UV treatment because there was a larger fold difference. After UV treatment, clone 10 did not show a reduction that was significant. This was likely due to the variance between the amplification that occurred in the samples during qRT-PCR. Because this strain had inconclusive results, phenotypic characterization of this strain was still conducted. Overall, Clone 1 was considered the most effective knock down strain.

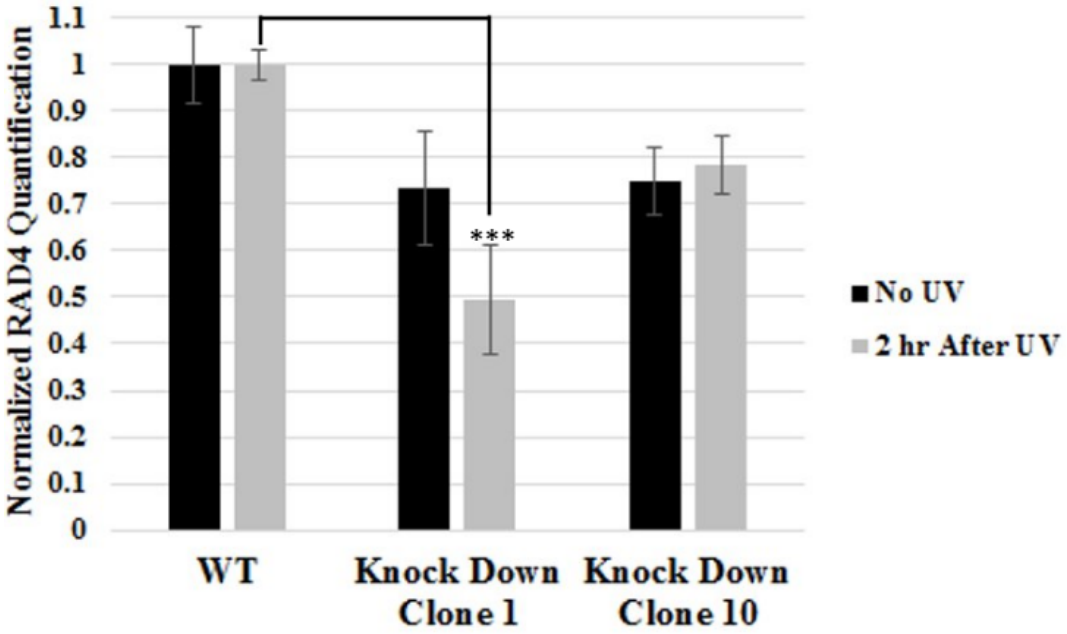

Figure 14. Quantification of *RAD4* Expression in the Knock Down Strains. *RAD4* expression was measured by qRT-PCR in wild type (WT; CU428), CU522 knock down clone 1, and CU522 knock down clone 10 either without UV exposure or following a two hour recovery after 100 J/m^2 UV light. Expression was normalized to *HHP1,* and made relative to wild type. Error bars represent +/- standard error of mean. *p value <0.05, **p value <0.01, ***p value <0.005 which were determined by a One-Way ANOVA with Tukey's HSDs. n=4.

Effect of UV and Hydrogen Peroxide on *Rad4* Knock Down Survivability

To begin examining the consequences of knocking down *Rad4,* the survival of these strains was measured after UV and hydrogen peroxide treatment. Comparing survival rates to wild type cells allowed for a measurement of how critical *RAD4* is when responding to genotoxic stressors. After UV treatment both knock down clones had decreased survival in comparison to wild type cells. Clone 1 had 56.66% and 26.76% reduced survival compared to wild-type after 75 and 100 J/m^2 UV treatments, respectively (Figure 15A). In clone 10, no significant differences in survival were detected, but for 50 and 100 J/m^2 UV an effect size was measured (Figure 15B). Based on the effect size, 92% after 50 J/m^2 and 78% after 100 J/m^2 UV treatment are due to the differences between the wild type and knock down strains. Overall, these results indicate that *RAD4* is involved in DNA repair mechanisms that allows for cell survival after UV damage.

Hydrogen peroxide treatment, which induces damage repaired by BER, was next used as a mutagenic agent to test *RAD4* activity. Clone 10 had a striking 94% decrease compared to wild type in survival after 0.5 mM hydrogen peroxide treatment (Figure 16). The decreases in survivability after both UV and hydrogen peroxide indicate the involvement of *RAD4* in both nucleotide excision repair and base excision repair.

Experimental Design and Optimization of DIG-labeled Telomere Probe Detection Assay

Probes against telomeric or sub-telomeric sequence often incorporate radioactive isotopes to detect telomere length in *T. thermophila* and other model organisms. An

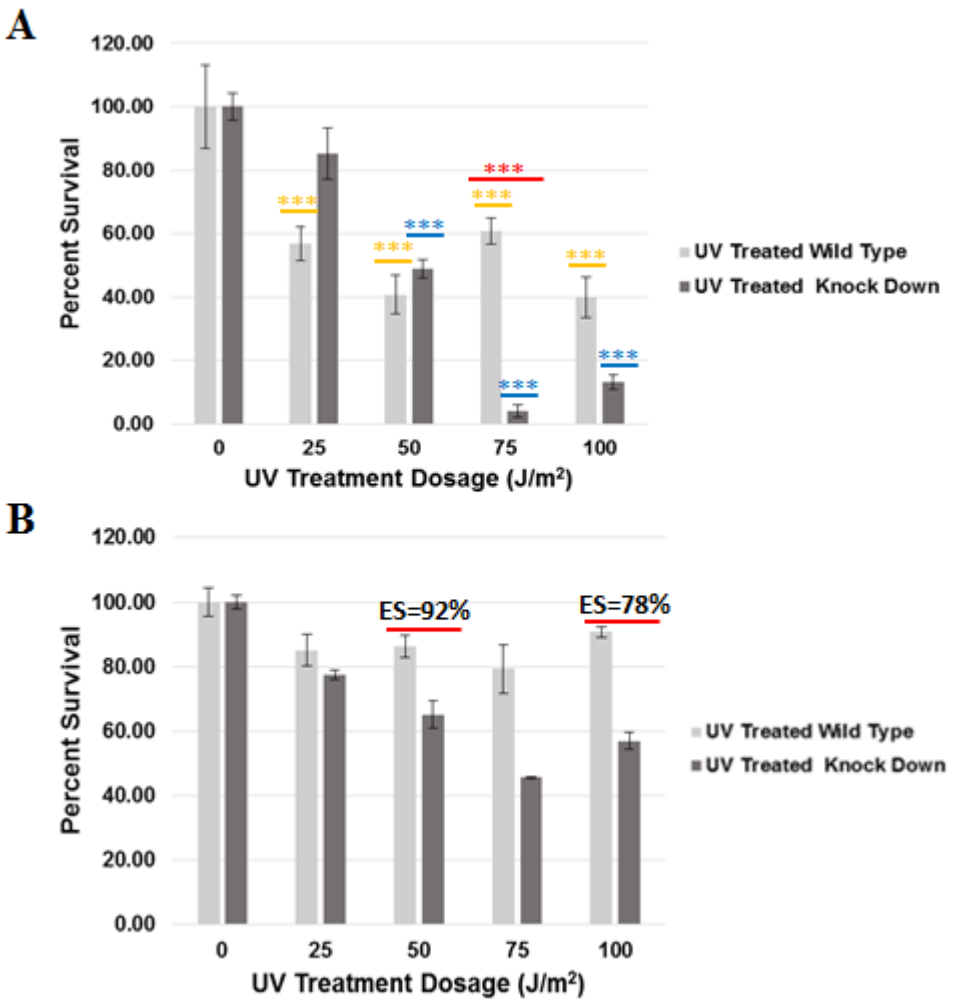

Figure 15. Effects of *Rad4* Knock Down on Survival After UV treatment. Survivability assay of three different possible *Rad4* knock down clones: (A) Clone 1, and (B) clone 10 were analyzed after various levels of UV treatment and compared to wild type. Samples were plated at approximately two cells per well in 96-well plates, and visualized for growth seven days later. 0 J/m^2 UV was considered 100% survival. Error bars represent +/- standard error of mean. ES indicates the effect size percentage. *p value <0.05, **p value <0.01, ***p value <0.005, determined by one-way ANOVA comparing untreated to each hour after treatment (orange: UV treated wild type; blue: UV treated knockdown), and comparing the same treatments (red). n=3.

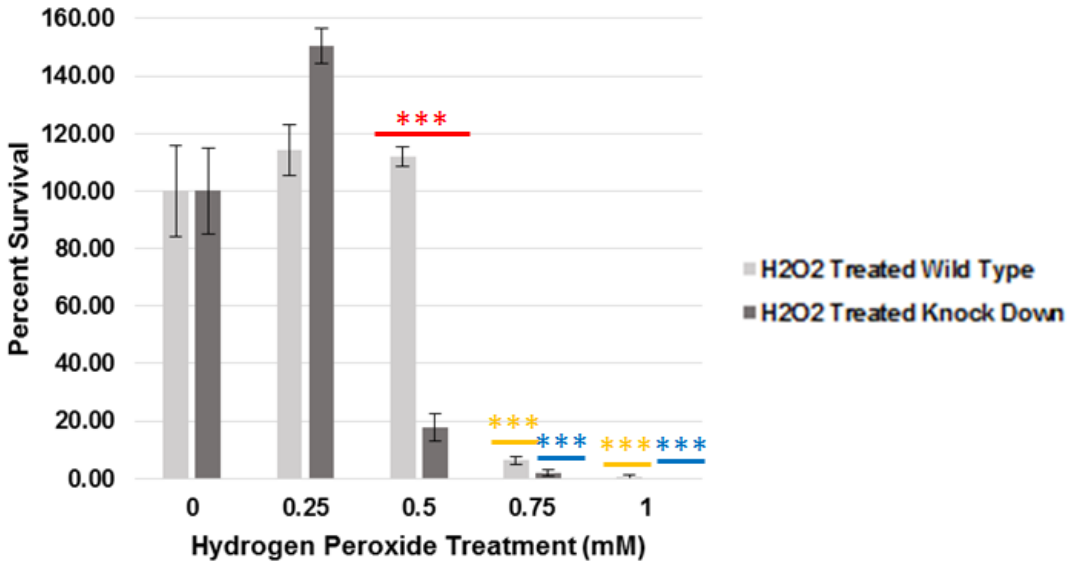

Figure 16. Effects of *Rad4* Knock Down on Survival after H_2O_2 Treatment. Survivability assays of *Rad4* knock down clone 10 were analyzed after various levels of hydrogen peroxide treatment (X-axis) and compared to wild type. Samples were plated at approximately two cells per well in 96-well plates, and visualized for growth seven days later. No hydrogen peroxide (0 mM) was considered 100% survival. Error bars represent +/- standard error of mean. *p value <0.05, **p value <0.01, ***p value <0.005 determined by one-way ANOVA comparing untreated to each hour after treatment (orange: UV treated wild type; blue: UV treated knockdown), and comparing the same treatments (red). n=3.

alternative probe used here contains telomeric sequence specific to *T. thermophila* but is conjugated to digoxigenin (DIG), which was then detected with a DIG specific antibody and eliminated the need for radioactive isotopes. Although DIG-labeling has been used in a wide variety of model organisms to detect telomere sequence, it has not been used in *T. thermophila*. Therefore, a novel assay was developed using DIG to detect telomere sequences (Figure 17A).

First, an efficient genomic DNA (gDNA) isolation protocol for *T. thermophila* was investigated. The traditional protocol lyses the cells with urea lysis buffer, two phenol chloroform extractions, and the DNA is precipitated through salt and isopropyl alcohol. Three variations of this traditional protocol were tested for efficiency. The first variation, "all", follows the traditional isolation process, but the entire protocol is conducted seamlessly in the same day. The second variation, "phenol", involved incubating the samples at -20°C overnight after the phenol extraction steps. The third variation, "pellet", involved removing the media from pelleted cells and incubating the pellet at 20°C overnight, and the remainder of the procedure was conducted the following day (Figure 18). Equal volumes of DNA isolated from each of the three methods were run on an agarose gel to compare the efficiency of DNA extraction from each method. More gDNA appeared to be isolated form the "phenol" method, than from "all" or "pellet", indicating that the phenol method was the most effective. All subsequence experiments were performed using the "phenol" method for gDNA extraction.

After the gDNA is isolated, the gDNA was fragmented and separated by agarose gel electrophoresis to prepare for blotting. The gDNA samples were digested with *Hind*III to release the telomeric sequence from the rest of the gDNA. The gDNA was

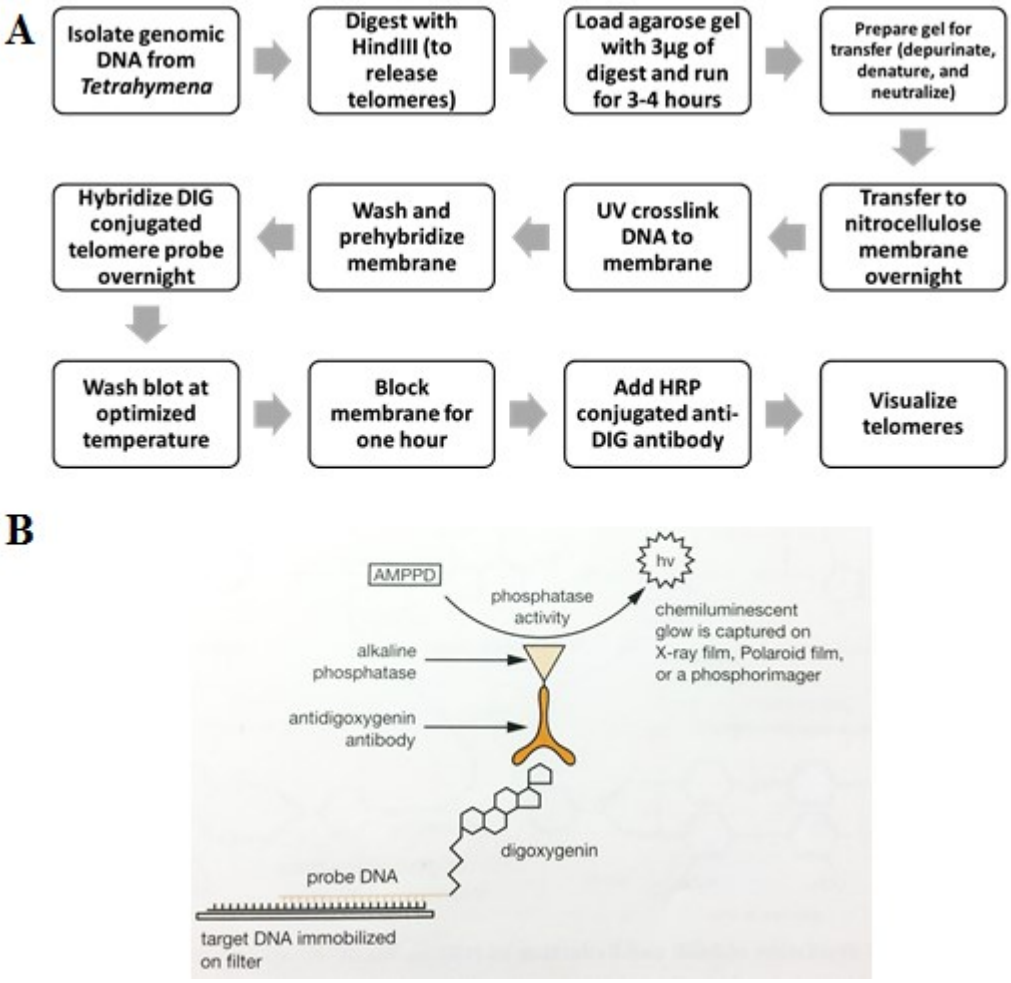

Figure 17. Development and Optimization of DIG-Labeled Telomere Probe Detection Assay. (A) This experimental schematic was developed to detect telomeric sequence without the use of a radioactive labeled probe. (B) A probe designed specifically for telomeric sequence in *T. thermophila* (GGGGTT) was conjugated to the digoxigenin (DIG) to be detected by a horseradish peroxidase (HRP) conjugated anti-DIG antibody. The antibody when reacted with hydrogen peroxide releases a chemiluminescent product which is detected on the blot (Sambrook and Russell, 2001).

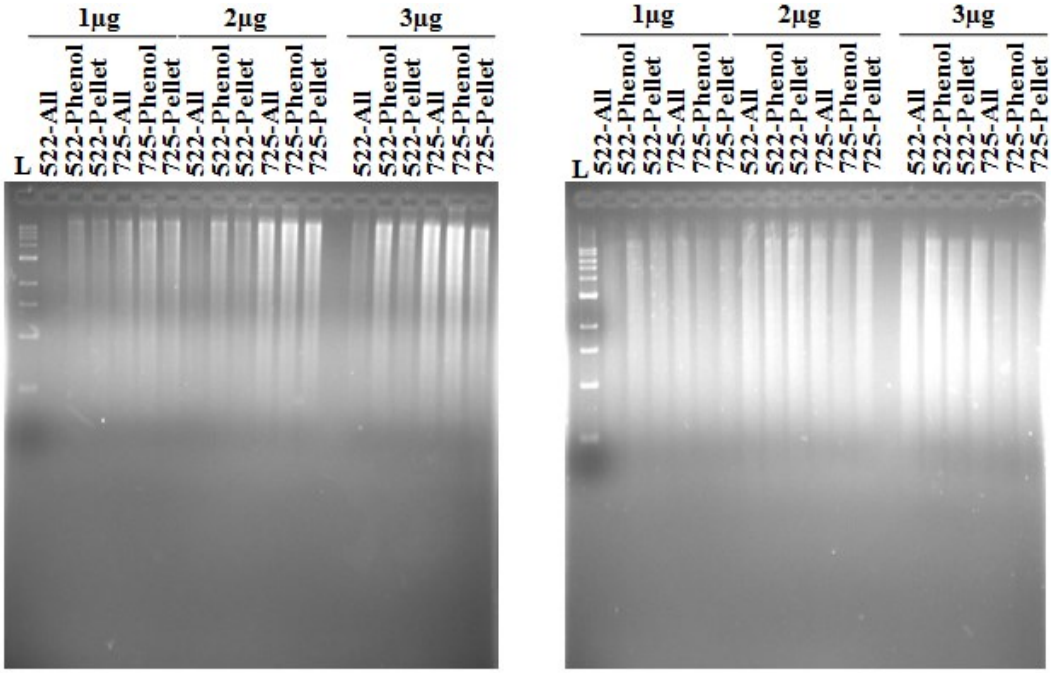

Figure 18. Optimization of gDNA Isolations for DIG-Labeled Telomere Probe Detection Assay. Digested genomic DNA samples from strains CU522 and CU725 were run on a 1.5% agarose gel in TBE. The samples were isolated with three protocol variation. "All" lanes contain samples isolated without any halt to the typical protocol. "Phenol" lanes contain samples stored at -20°C overnight after the two phenol extractions, and then the isolation was completed. "Pellet" lanes contain samples that the cells were pelleted and then stored at -20°C overnight before continuing the isolation. The experiment was done in duplicate to allow for more conditions to be tested for optimization.

separated by agarose gel electrophoresis at a low voltage (70 V) over three to four hours, to maximize separation. An agarose gel was loaded with one, two, and three µg of DNA, and at least three µg was used in subsequent gels. The initial test showed more intensity than subsequent experiments (data not shown). The predicted issue with this was the use of different Nanodrop spectrophotometers. The Nanodrop 2000 gave consistently higher readings than the ImplenNanoPhotometer NP80, therefore, less DNA was digested and ran on the gel when read with the Nanodrop 2000. This issue was resolved by use of the ImplenNanoPhotometer NP80 for sample analysis, and five µg of DNA.

To prepare the blot, the agarose gels were transferred to nitrocellulose membrane and crosslinked. The gels were stained with ethidium bromide prior to transfer, in order to estimate amounts of DNA per lane. The blot was prepared for hybridization by a pre-hybridization incubation that prevents non-specific binding of the probe to the membrane. The DIG-labeled telomeric probe was hybridized to the blot overnight by incubating at a temperature at least 42°C. After hybridization, the blot was washed to remove non-specifically bound probe from the membrane. Different wash temperatures were tested (42, 45, and 50°C) and optimal signal was detected at 45°C, therefore, this temperature was used in future assays (Figure 19).

Next, the blot was blocked, then incubated with the anti-DIG antibody (Figure 17B). Optimization of antibody detection occurred by varying blocking agents and antibody concentration. Li-cor blocking agent and 0.5% milk in TBST were tested for their blocking ability. 0.5% milk in TBST allowed optimal signal and thus was used in future assays (Figure 19). The anti-DIG antibody conjugated to horseradish peroxidase was added in 1:500 and 1:1000 dilutions. The 1:1000 dilution showed an optimal signal,

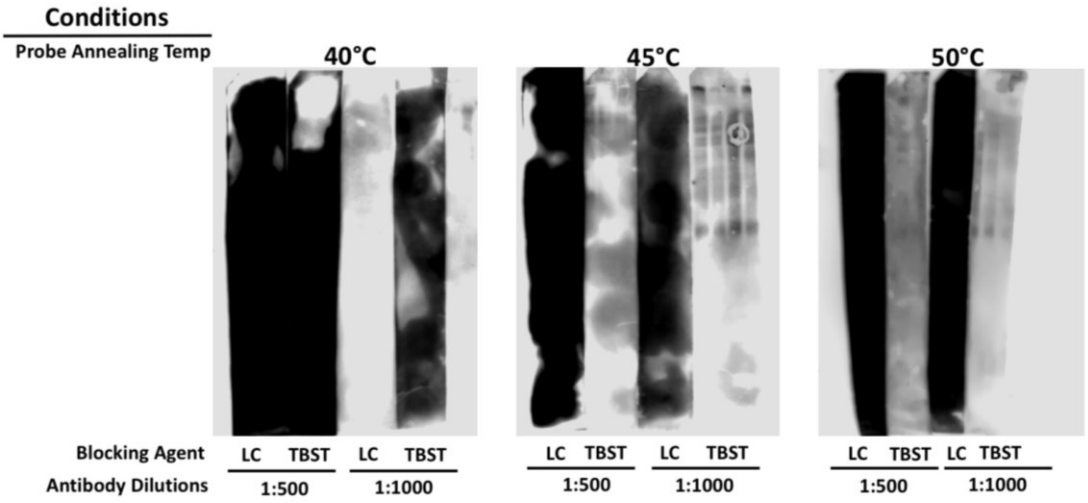

Figure 19. Optimization of Blotting Conditions for DIG-Labeled Telomere Probe Detection Assay. Strips of membrane with digested genomic DNA were treated with a variety of conditions to find the optimal combination for future assays. The values listed above the nitrocellulose membranes are the varying temperatures used for the wash directly following overnight probe hybridization at 42°C. Li-Cor blocking agent (LC) and 0.5% Milk in TBST (Milk) served as antibody blocking agents. The 1:500 and 1:1000 indicate the anti-DIG antibody dilutions.

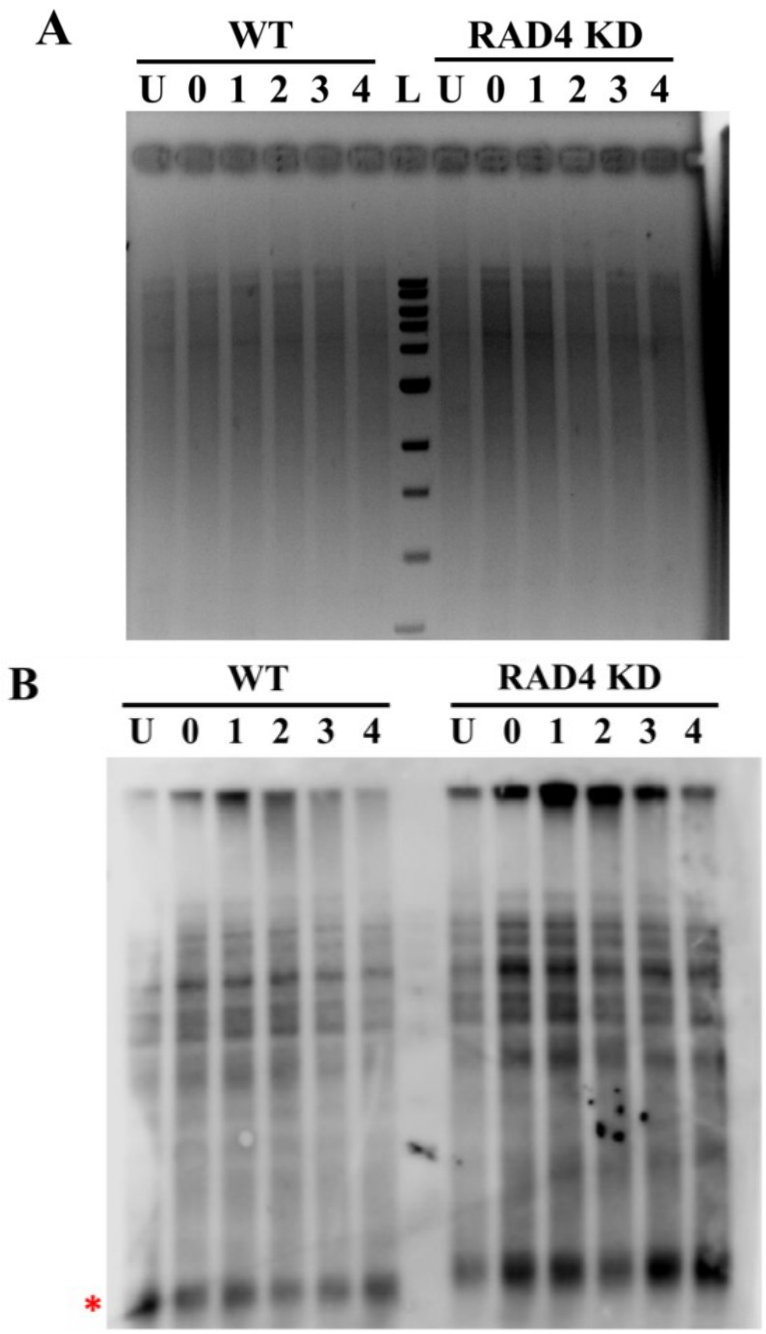

Figure 20. Telomere Detection in Wild Type and *Rad4* Knock Down Strains. Digested samples of genomic DNA isolated from wild type cells (WT; CU428) and *Rad4* knock down clone 1 (KD). Both samples were treated with 100 J/m^2 UV and were allowed to recover for four hours. Samples were isolated before treatment (U), immediately after treatment (0), one to four hours after treatment (1-4). Lane L contains a 1KB ladder. (A) Samples were first run on 1.5% agarose TAE gel. (B) Then samples were blotted to the nitrocellulose membrane and the DIG probe conjugated to *T. thermophila* telomere sequence. Red star indicates band quantified for telomere length analysis.

and was used in future assays (Figure 17B and Figure 19). The membrane was then exposed to SuperSignal West Dura Stable Peroxide Buffer and SuperSignal West Dura Lumino/Enhancer Solution, and was visualized using both the LI-COR Odyssey FC and the Agfa CP1000 Automatic Film Processor. Although the LI-COR required a longer amount of exposure to acquire comparable images to the film processor (data not shown), the LI-COR images were able to achieve a quality image (Figure 19 and 20).

Telomere Length in *Rad4* Knock Down Strain

The optimized DIG-labeled telomere probe detection assay was used to characterize the differences in telomere composition between wild type (WT) and a *Rad4* knock down strain (RAD4 KD). Telomeres from both untreated and UV treated samples from wild type cells and *Rad4* knock down clone 1 were analyzed. UV treated cells were exposed to 100 J/m^2 UV, and allowed to recover for four hours. Genomic DNA (5 µg) was loaded onto an agarose gel and electrophoresed (Figure 20A).

After samples were transferred to a nitrocellulose membrane, telomeres were visualized with the anti-DIG antibody. As expected, multiple bands show a heterogeneous mixture of telomere sizes. Probing of this blot for actin 1 as a loading control was also attempted. Unfortunately, it appears that more optimal probe design or conditions need to be made for this probe as no detection was possible (data not shown). In place of this loading control, gDNA streak intensity was quantified and used for normalization (Figure 20A). The intensity of the lowest band on the nitrocellulose membrane, likely representative of the telomeres on rDNA minichromosomes, was

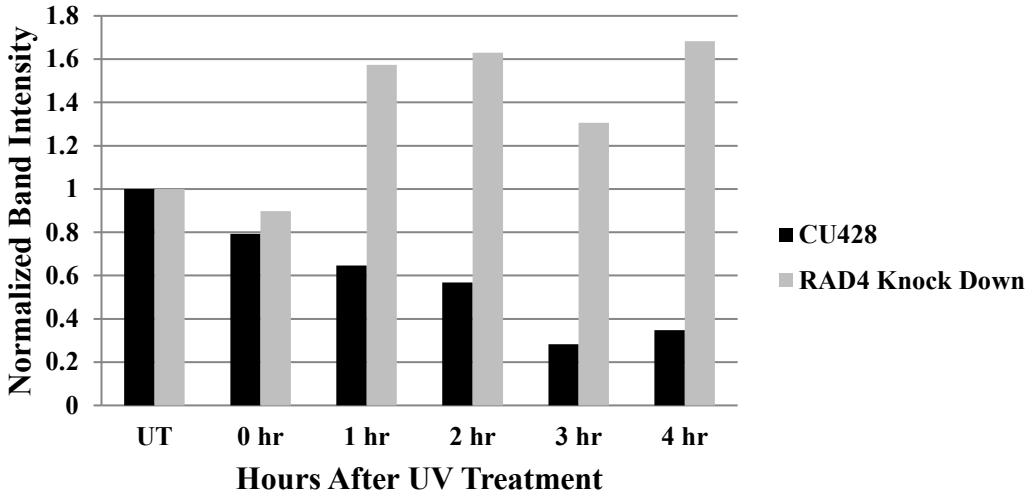

Figure 21. Telomere Quantification in Wild Type and RAD4 Knock Down Strains. Quantification of the intensity of rDNA minichromosome band on nitrocellulose membrane (marked with red star Figure 20B). Samples were normalized to genomic streak intensity on the agarose gel (Figure 20A), and made relative to untreated (UT). n=1.

measured as a representative telomere length for the cell (Figure 20B, indicated with a red star). The intensity of this band indicates the number of telomeric repeats of rDNA minichromosomes (Figure 21). After UV treatment, the telomeres in the wild type gradually decrease in size after UV treatment, while the *Rad4* knock down strain telomeres increase in size after UV treatment. At the end of the time course a 0.35 relative decrease and 1.68 relative increase respectively occurred in telomere length. This indicated that *RAD4* regulates telomere length in *T. thermophila*.

DISCUSSION

The Role of *RAD4* in NER and BER

The overall purpose of this research is to understand the role of *RAD4* in DNA repair and its interplay with telomeres in *Tetrahymena thermophila.* It was anticipated that, due to telomeres unique structure, nucleotide excision repair would occur differently than in other areas of the genome. Analysis of the proteins associated with telomeres (shelterin) revealed that overall shelterin proteins did not possess a large amount of sequence conservation between organisms (Table 3). This lack of conservation makes it challenging to find translatable results between organisms. The only detectable common domains in the shelterin proteins in T. thermophila are Pot1a and Tpt1. However, XPC/Rad4 proteins have strong conservation of the beta hair pin domain 1-3 and transglutaminase domain, and are an attractive point of study between *T. thermophila* and more complex model organisms (Table 4, Figure 5).

RAD4 expression levels in *T. thermophila* were measured after exposure to DNA damaging agents (UV, H_2O_2 and MMS) to determine the involvement of Rad4 in DNA repair (Figure 9). *RAD4* expression significantly increases after both UV and hydrogen peroxide treatment then gradually decreases, a typical expression pattern for DNA repair genes, which expression spikes in response to the damage and then begins to return to basal levels (Ramsey et al., 2004; Joshua Smith, unpublished data; Figure 9D). Previously *RAD4* has been implicated in the recognition of damage in global genome nucleotide excision repair in response to UV damage (Evans et al., 1997). Rad4 also plays a role in base excision repair by binding Ogg1, the base excision repair damage

recognition protein, and increasing the affinity of Ogg1 to damage (Melis et al., 2013). At their peaks, *RAD4* expression levels after UV and hydrogen peroxide treatment rose 129- and 108-fold, respectively. These drastic increases in *RAD4* expression in response to UV and oxidative damage are likely related to its role in nucleotide excision repair (NER) and base excision repair (BER) in *T. thermophila.* These findings validate *T. thermophila* as a model organism in the study of NER and BER.

Rad4 Knock Down Reveals Important Role in NER and BER

Rad4 levels were depleted in *Tetrahymena* to further characterize its role in NER and BER through stable short hair pin RNA construct (Figure 10). Knock down of *Rad4* was confirmed in these strains through measurement of *RAD4* expression levels by qRT-PCR (Figure 14). There was a significant reduction (51%) in *Rad4* transcription levels in clone 1, indicating successful knock down of *Rad4* by the shRNA. Although not significant, there was an apparent reduction in expression levels in clone 10. The lack of significance is likely due to the variances between the amplification of samples during qRT-PCR.

Survivability after mutagenic treatment was used to measure the ability of *T. thermophila* to repair the DNA damage, rather than enter apoptosis. UV treatment decreased survivability upon *Rad4* depletion, indicating that *T. thermophila* are not able to repair UV-induced DNA damage with NER (Figure 15A). Clone 10 showed insignificant results in both expression reduction and UV treatment. Interestingly, survivability appeared to be dose dependent, as knock down clone 1 had more reduction in survivability than clone 10, where *Rad4* knock down and survivability after UV was

reduced, but not significant. Knock down clone 10 had significantly decreased survivability after hydrogen peroxide treatment (Figure 16), indicating that even subtle *Rad4* depletion has dramatic impacts on the BER pathway. Altogether, *T. thermophila* Rad4 likely contributes to the ability of NER and BER system to recognize damage and recruit the additional proteins needed to repair the damage. When *Rad4* is absent, the damage accumulates, and the cells enter apoptosis.

Development of a DIG-Labeled Telomere Probe Detection Assay

The establishment of an assay to measure telomere length via a DIG-labeled telomere-specific probe was a cornerstone of this project (Figure 17). The ability to work with radioactive isotopes is limited to institutions or scientists with the facilities, equipment, clearance and training to do so, therefore the ability to detect telomeres without radioactive labeled probes should open telomere biology studies to a wider range of institutions and laboratories.

The design of DIG-based telomere detection required the collaboration of many resources and scientists. Dr. Benjamin Linger was consulted on the length and possible sequence of the probe, and telomere isolation techniques. The blotting and probing protocol was combined from different resources, including those contributed by Dr. Smith, Dr. Ulbricht, and a variety of biotechnical companies that have DIG labeling products. Time and effort was devoted to understanding current radiolabeled methods of telomere detection in *T. thermophila* previous work of from Dr. Carolyn Price and Dr. Linger. Considerations from these sources helped develop the ideal conditions for probe

design, gDNA isolation, hybridization, blotting, probe detection, and interpretation of the results from the telomere detection assay.

While designing the DIG-based telomere detection assay, steps of the protocol were identified as potential targets of optimization as the procedure was refined. Three different gDNA isolation conditions were attempted, and the technique with the most intense gDNA streak on an agarose gel after *Hind*III digestion was selected (Figure 18). Phenol chloroform extraction and ethanol precipitation in one day from freshly isolated cells or those pelleted frozen overnight was inferior to performing two consecutive phenol chloroform extractions on freshly isolated cells and freezing the aqueous layer overnight before precipitation the next day. The key difference between these protocols is likely the freeze-thaw step that may increase the solubility of DNA.

After optimization of the gDNA isolation procedure, multiple hybridization and blotting conditions for probing and detection were considered (Figure 19). The wash temperatures after hybridization of the probe were varied from 42°C to 50°C. The most distinctive telomeric banding was seen at 45°C, suggesting that this temperature allows optimal removal of background, without disrupting interaction between the probe and gDNA. Detection of the DIG-labeled probe was optimized by varying the blocking agent and anti-DIG antibody concentration (Figure 19). Li-cor blocking solution seemed to be ineffective since the image of the blot was completely dark at all washing temperatures and antibody concentrations, with no distinct bands. Blocking in 0.5% milk in TBST allowed distinct bands to appear in lanes with gDNA, indicating that this condition is optimal for allowing binding of the anti-DIG antibody to the DIG-labeled probe, but preventing non-specific binding of the antibody to the blot. Incubation of the blot in

1:1000 anti-DIG antibody resulted in clearer bands on the blot than in a 1:500 dilution of the antibody, suggesting that incubation of the blot in the more dilute concentration of antibody is optimal for probe detection. Altogether, the washing step at 45°C, the antibody in a 1:1000 dilution, and the blocking buffer of 0.5% milk in TBST made optimal conditions for probe washing and detection.

The Effect of *RAD4* on Telomeres

With the DIG-labeled telomere probe detection assay optimized, telomeres from wild type and *Rad4* knock down *T. thermophila* were analyzed to determine the effects of depleted *Rad4* levels on telomere composition (Figure 20 and 21). In tandem with telomere detection, a actin probe was designed to be used, providing an internal control for the amount of gDNA in each lane. Unfortunately, the actin probe had no discernable bands, indicating that probe design, hybridization, or washing conditions need to be further optimized. Instead, an alternative loading control was developed where gDNA amount was quantified from ethidium bromide stains of each gel, prior to blotting (Figure 20A). Telomeres on rDNA minichromsome were selected for quantification by measuring the intensity of the band, which is an indication of the amount of telomere repeats (indicated by a red star; Figure 20B). After UV exposure, the *Rad4* knock down clone 1 has longer telomeres than wild type strain (Figure 21). This is consistent with previous literature which showed that XPC knock outs resulted in longer telomeres after UV exposure in *Mus musculus* (Stout and Blasco, 2013). In wild type cells, UV exposure leads to shortened telomeres, whereas cells that are deficient in XPC, which are also

deficient in NER and BER, actually extend telomeres after UV exposure, which has also been supported in the literature (Ramírez et al., 2002).

The *Rad4* depletion in *T. thermophila* potentially stresses the cells stimulating alternative lengthening of the telomeres. This mechanism helps to add telomeric sequence when the cells are under duress. Alternatively, the presence of unrepaired pyrimidine dimers could be hypothesized to cause shelterin proteins to not bind as effectively to the damaged DNA. Since shelterin proteins block telomerase access to the telomeres, disrupting their binding leads to aberrant lengthening of telomeres (Palm and de Lange, 2008). It is evident that Rad4 in *T. thermophila* plays a critical role in length regulation and telomere maintenance.

Future Directions

This work contributes a significant step forward in our understanding of the interactions of Rad4, and more generally DNA repair, and telomere regulation. Moreover, the work opens a wide-range of avenues for future studies. To more completely verify *Rad4* knock down clone 1 and 10 are depleting the protein as well as the transcript after UV and hydrogen peroxide treatments, GFP or RFP tagged *RAD4* could be transformed in the rlp29 locus and visualized. Additionally, creating a complete knock out of *RAD4* would allow for clear characterization of cells without the function in NER and telomere repair.

Further phenotypic characterization of *Rad4* knock downs may clarify the conclusions made here or provide additional information. Specifically, hydrogen peroxide treatment of the most significantly affected *Rad4* knock down (clone 1) is

expected to produce an even more pronounced reduction in survivability after hydrogen peroxide treatment. Also, an increase in the amount of UV survivability assays will increase the power of the experiment and determine if the interesting, yet not statistically significant, observed effects between the wild type and *Rad4* knock downs were due to variability in the assay or sample, or due to subtle effects of the inefficient *Rad4* knock down.

Only one telomere assay was able to be performed since a large amount of time and resources were spent on development of the assay. Additional trials of this telomere detection assay will allow statistical analysis of the telomere length and strengthen the conclusions made in this one impressive experiment. It would also be interesting to compare telomere lengths in both clone 1 and clone 10, to see if the knock down efficiency effects telomere length. Since this study consistently shows Rad4-dependent BER phenotypes, it would be interesting to see the effects on telomere composition after hydrogen peroxide treatment. Previous studies have shown that telomeres shorten after hydrogen peroxide treatment (Ting et al., 2010). After hydrogen peroxide treatment, it is possible we would observe a very similar phenotype after UV treatment, but if there is a lack of change it would show NER specificity. Also, it would be advantageous to extend the time course for the gDNA isolations until telomere lengths return to untreated levels.

Importantly, this study provides Missouri State University and other institutions with the ability to study telomeres without radioactive labeled probes. An interesting augmentation to this protocol could be using a probe to the subtelomeric region, rather than the telomere repeat. These studies have been performed by the Price lab with forward and reverse radioactive labeled probes specific to the subtelomeric sequence of

specific telomeres in *T. thermophila* (Jacob et al., 2004). The advantage of this design is a potentially cleaner blot, showing specific telomere length, instead of a heterogeneous mixture of telomeres. An internal rDNA probe on the minichromosome could be used for normalization. Additionally, the optimization of the actin probe would be another effective loading control that could be optimized as an appropriate loading control.

At the genesis of this project, there were hopes of obtaining a variety of tagged strains from the Price lab. The particular strains of interest we would have liked to have studied. The likely most important is the TERT knockout construct and strain (Linger et al., 2011). This would serve as an excellent control for cells that would have shorter telomeres. The overall ultimate goal of this research is to find a potential shelterin binding partner to RAD4. Because this is a recognition protein that would be the first to interact with damaged telomeric DNA, a binding partner could be expected (Jia et al., 2015). To study this interaction there are two possible approaches, co-immunopercipitation of tagged Rad4 or tagged shelterin proteins. Currently the Price lab has POT2-HA, POT1-TAP, and TPT1-TAP (Cranert et al., 2014; Jacob et al., 2007; Linger et al., 2011). Because currently tagging Rad4 has proven problematic (Emily Nischwitz and Rachel Mullner unpublished data), it would be beneficial to acquire those tagged strains for further studies. Additionally, knockout strains of POT2, POT1, and TPT1 also have shown interesting length phenotypes that could be studied with the newly establish DIG-labeled probe telomere detection assay (Cranert et al., 2014; Jacob et al., 2007; Linger et al., 2011).

Overall, this project added resources to the scientific community to be able to study DNA repair and telomere biology. The establishment of characterized *Rad4* knock

down strains allow researchers to continuing the study of NER in *T. thermophila* within the macronucleus and micronucleus. Additionally, the newly established DIG-labeled telomere probe detection assay allows for *Tetrahymena* labs to be able to study telomere length and composition in the context of DNA repair and any other field.

.

REFERENCES

Alter, B.P., Giri, N., Savage, S.A., and Rosenberg, P.S. (2009). Cancer in dyskeratosis congenita. Blood *113,* 6549-6557.

Altschul, S.F., Stephen, F., Madden, T.L., Schäffer, A.A., Zhang, J., Zhang, Z., Miller, W., and Lipman, D.J. (1997). Gapped BLAST and PSI-BLAST: a new generation of protein database search programs. Nucleic Acids Res. *25,* 3389-3402.

Armanios, M. (2012). Telomerase and idopathic pulmonary fibrosis. Mutat. Res. *730,* 52-58.

Bass, H.W., Marshall, W.F., Sedat, J.W., Agard, D.A., and Cande, W.Z. (1997). Telomeres cluster de novo before the initation of synapsis: a three-dimensional spatial analysis of telomere positions before and during meiotic phrophase. J. Cell Biol. *137,* 5-18.

Bauman, P., and Cech, T.R. (2001). Pot1, the putative telomere end-binding protein in fission yeast and humans. Science *292,* 1171-1175.

Bianchi, A., Smith, S., Chong, L., Elias, P., and de Lange, T. (1997). TRF1 is a dimer and bends telomeric DNA. EMBO. *18,* 5735-5744.

Blackburn, E.H., Budarf, M.L., Challoner, P.B., Cherry, J.M., Howard, E.A., Katzen, A.L., Pan, W.C., and Ryan, T. (1983). DNA termini in ciliate macronuclei. Quant. Biol. *47,* 1195-1207.

Blackburn, E.H., and Gall, J.G. (1978). A tandemly repeated sequence at the termini of the extrachromosomal ribosomal RNA genes in *Tetrahymena.* J. Mol. Biol. *120*, 33-53.

Boswell, R.E., Klobutcher, L.A., and Prescott, D.M. (1982). Inverted terminal repeats are added to genes during macronuclear development in *Oxytricha nova.* Proc. Natl. Acad. Sci. USA. *79,* 3255-3259.

Broccoli, D., Smogorzewska, A., Chong, L., and de Lange, T. (1997). Human telomeres contain two distinct Myb-related proteins, TRF1 and TRF2. Nat. Genet. *17,* 231-235.

Bunick, C.G., Miller, M.R., Fuller, B.E., Fanning, E., and Chazin, W.J. (2006). Biochemial and structural domain analysis of xeroderma pigmentosum complementation group C protein. Biochem. *45,* 14965-14979.

Cranert, S., Heyse, S., Linger, B., Lescasse, R., and Price, C. (2014). *Tetrahymena* Pot2 is a developmentally regulated paralog of Pot1 that localizes to chromosome breakage sites but not to telomeres. Eukaryot. Cell *13*, 1519-1529.

Celli, G., and de Lange, T. (2005). DNA processing not required for ATM-mediated telomere damage response after TRF2 depletion. Nat. Cell Biol. *7,* 712-718.

Cesare, A.J., and Reddel, R.R. (2010). Alternative lengthening of telomeres: models, mechanisms and implications. Nat. Rev. Genet. *11,* 319-330.

Cleaver, J.E. (1968). Defective repair replication of DNA in xeroderma pigmentosum. Nature *218*, 652-656.

Cleaver, J.E. (2005). Cancer in xeroderma pigmentosum and related disorder of DNA repair. Nat. Rev. Cancer *5*, 564-573.

Coin, F., Oksenych, V., Mocquet, V., Groh, S., Blattner, C., and Egly, J.M. (2008). Nucleotide excision repair drive by the dissociation of CAK from TFIIH. Mol. Cell *31,* 9-20.

Cooper, J.P., Nimmo, E.R., Allshire, R.C., and Cech, T.R. (1997). Regulation of telomere and function by a Myb-domain protein in fission yeast. Nature *385,* 744-747.

DiGiovanna, J.J., and Kraemer, K.H. (2012). Shining a light on xeroderma pigmentosum. J. Invest. Dermatol. *132,* 785-796.

de Laat, W.L., Appeldoorn, E., Sugasawa, K., Weterings, E., Jaspers, N.G., and Hoeijmakers, J.H. (1998). DNA-binding polarity of human replication protein A positions nucleases in nucleotide excision repair. Genes Dev. *12,* 2598-2609.

Dokal, I. (2000). Dyskeratosis congenital in all its forms. Br. J. Haematol. *110,* 768-779.

Evans, E., Moggs, J.G., Hwang, J.R., Egly, J.M., and Wood, R.D. (1997). Mechanism of open complex and dual incision formation by human nucleotide excision repair factors. EMBO J. *16,* 6559-6573.

Fagbemi, A.F., Orelli, B., and Schärer, O.D. (2011). Regulation of endonuclease activity in human nucleotide excision repair. DNA Repair *10,* 722-729.

Fan, J., and Pavletich, N.P. (2012). Structure and conformational change of a replication protein A heterotrimer bound to ssDNA. Genes Dev. *26,* 2337-2347.

Finn, R.D., Attwood, T.K., Babbitt, P.C., Bateman, A., Bork, P., Bridge, A.J., Chang, H-Y., Dosztanyi, Z., El-Gebali, S., Fraser, M., et al. (2017). InterPro in 2017-beyond protein family and domain annotations. Nucleic Acids Res. *45,* D190-D199

Flory, M.R., Carson, A.R., Muller, E.G., and Aebersold, R. (2004). An SMC-domain protein in fission yeast links telomeres to the meiotic centrosome. Mol. Cell *16,* 619-630.

Gao, H., Cervantes, R.B., Mandel, E.K., Otero, J.H., and Lundblad, V. (2007). RPA-like proteins mediate yeast telomere function. Nat. Struct. Mol. Biol. *14,* 208-214.

Gillet, L.C., and Schärer, O.D. (2006). Molecular mechanisms of mammalian global genome nucleotide excision repair. Chem. Rev. *106,* 253-276.

Gilljam, K.M., Muller, R., Liabakk, N.B., and Otterlei, M. (2012). Nucleotide excision repair is associated with the replisome and its efficiency depends on a direct interaction between XPA and PCNA. PloS ONE *7,* e49199

Gillooly, J.F., Hein, A., and Damiani, R. (2015). Nuclear DNA content varies with cell size across human cell types. Cold Spring Harb. Perspect. Biol. *7,* a019091.

Gopalakrishnan, K., Low, G.K.M., Ting, A.P.L., Srikanth, P., Slijepcevic, P., and Hande, M.P. (2010). Hydrogen peroxide induced genomic instability in nucleotide excision repair-deficient lymphoblastoid cells. Genome Integrity *16,* 1-14.

Greider, C.W., and Blackburn, E.H. (1985). Identification of a specific telomere terminal transferase activity in *Tetrahymena* extracts. Cell *43,* 405-413.

Griffith, J.D., Comeau, L., Rosenfield, S., Stansel, R.M., Bianchi, A., Moss, H., and de Lange, T. (1999). Mammalian telomeres end in a large duplex loop. Cell *97,* 503-514.

Hanawalt, P.C., and Spivak, G. (2008). Transcription-coupled DNA repair: two decades of progress and surprises. Nat. Rev. Mol. Cell Biol. *9,* 958-970.

Henderson, E., Hardin, C.C., Walk, S.K., Tinoco, I., and Blackburn, E.H. (1987). Telomeric DNA oligonucleotides form novel intramolecular structures containing guanine-guanine base pairs. Cell *51,* 899-908.

Henderson, E.R., and Blackburn, E.H. (1989). An overhang 3` terminus is a conserved feature of telomeres. Mol. Cell Biol. *9,* 345-348.

Hirano, Y., Fukunaga, K., and Sugimoto, K. (2009). Rif1 and rif2 inhibit localization of tel1 to DNA ends. Cell *126,* 63-77.

Hohl, M., Thorel, F., Clarkson, S.G., and Schärer, O.D. (2003). Structural determinants for substrate binding and catalysis by the structure-specific endonuclease XPG. J. Biol. Chem. *278,* 19500-19508.

Jacob, N.K., Stout, A.R., and Price, C.M. (2004). Modulation of telomere length dynamics by the subtelomeric region of *Tetrahymena* telomeres. Mol. Biol. of the Cell *15,* 3719-3728.

Jacob, N.K., Lescasse, R., Linger, B.R., and Price, C.M. (2007). *Tetrahymena* POT1a regulates telomere length and prevents activation of a cell cycle checkpoint. Mol. Cell Biol. *27*, 1592-1601.

Jia, P., Her, C., and Chai, W. (2015). DNA excision repair at telomeres. DNA Repair (Amst.) *36.* 137-145.

Kanoh, J., and Ishikawa, F. (2001). spRap1 and spRif1, recruited to telomeres by Taz1, are essential for telomere function in fission yeast. Curr. Biol. *11,* 1624-1630.

Katzen, A.L., Cann, G.M., and Blackburn, E.H. (1981). Sequence specific fragmentation of macronuclear DNA in a holotrichous ciliate. Cell *24,* 313-320.

Kelleher, C., Kurth, I., and Linger, J. (2005). Human protection of telomeres 1 (POT1) is a negative regulator of telomerase activity in vitro. Mol. Cell Biol. *25,* 808-818.

Kumar, S., Stecher, G., and Tamura, K. (2016). MEGA7: Molecular Evolutionary Genetic Analysis Version 7.0 for bigger datasets. Mol. Biol. Evol. *33,* 1870-1874.

Klobutcher, L.A., Swanton, M.T., Donini, P., and Prescott, D.M. (1981). All gene-sized DNA molecules in four species of hypotrichs have the same terminal sequence and an unusual 3` terminus. Proc. Natl. Acad. Sci. USA. *78,* 3015-3019.

Kocak, H., Ballew, B.J., Bisht, K., Eggebeen, R., Hicks, B.D., Suman, S., O'Neil, A., Giri, N., Maillard, I., Alter, B.P., et al. (2014). Hoyeraal-Hreidarsson syndrome caused by a germline mutation in the TEL patch of the telomere protein TPP1. Genes Dev. *28,* 2090-2102.

Lazzerini-Denchi, E. and Sfeir, A. (2016). Stop pulling my strings-what telomeres taught us about the DNA damage response. Nat. Rev. Mol. Cell Biol. *17,* 364-378.

Lehmann, A.R. (2003). DNA repair-deficient diseases, xeroderma pigmentosum, Cockayne syndrome and trichothiodystrophy. Biochimie *85,* 1101-1111.

Lei, M., Podell, E.R., and Cech, T.R. (2004). Structure of human POT1 bound to telomeric single-stranded DNA provides a model for chromosome end-protection. Nat. Struct. Mol. Biol. *11,* 1223-1229.

Li, B., Oestreich, S., and de Lange, T. (2000). Identification of human Rap1: implications for telomere evolution. Cell *101,* 471-483.

Li, L., Elledge, S.J., Peterson, C.A., Bales, E.S., and Legerski, R.J. (1994). Specific association between the human DNA repair proteins XPA and ERCC1. Proc. Natl. Acad. Sci. *91,* 5012-5016.

Li, W., Cowley, A., Uludag, M., Gur, T., McWilliam, H., Squizzato, S., Park, Y.M., Buso N., and Lopez, R. (2015). The EMBL-EBI bioinformatics web and programmatic tools framework. Nucleic Acids Res. *43,* W580-W584.

Linger, B.R., Morin, G.B., and Price, C.M. (2011). The Pot1a-associated proteins Tpt1 and Pat1 coordinate telomere protection and length regulation in *Tetrahymena.* MBoC. *22*, 4161-4170.

Marcand, S., Gilson, E., and Shore, D. (1997). A protein-counting mechanism for telomere length regulation in yeast. Science *275,* 986-990.

McClintock, B. (1931). Cytological observation of deficiencies involving known genes, translocations and inversion in *Zea mays.* Missouri Agr. Exp. Sta. Res. Bull. *163,* 1-48.

Melis, J.P.M., van Steeg, H., and Luijten, M. (2013). Oxidative DNA damage and nucleotide excision repair. Antioxidants and Redox Signaling. *18,* 2409-2419.

Min, J.H., and Pavletich, N.P. (2007). Recognition of DNA damage by the Rad4 nucleotide excision repair protein. Nature *499,* 570-575.

Mitchell, J.R., Wood, E., and Collins, K. (1999). A telomerase component is defective in the human disease dyskeratosis congenital. Nature *402,* 551-555.

Morin, G.B. (1989). The human telomere terminal transferase enzyme is a ribonucleoprotein that synthesizes TTAGGG repeats. Cell *59,* 521-529.

Moser, J., Kool, H., Giakzidis, I., Caldecott, K., Mullenders, L.H., and Fousteri, M.I. (2007). Sealing of chromosomal DNA nicks during nucleotide excision repair requires XRCCI and DNA ligase III α in a cell-cycle-specific manner. Mol. Cell *27,* 311-323.

Moyzis, R.K., Buckingham, J.M., Cram, L.S., Dani, M., Deavn, L.L., Jones, M.D., Meyne, J., Ratliff, R.L., and Wu, J.R. (1988). A highly conserved repetitive DNA sequence (TTAGGG)n, present at the telomeres of human chromosomes. Proc. Natl. Acad. Sci. USA. *85,* 6622-6626.

Mullner, H.J. (1938). The remaking of chromosomes. Collecting Net*. 13,* 181-198.

Notredame, C., Higgins, D.G., and Heringa, J. (2000). T-Coffee: A novel method for fast and accurate multiple sequence alignment. J. of Mol. Biol. *302,* 205-217.

Ogi, T., and Lehmann, A.R. (2006). The Y-family DNA polymerase kappa functions in mammalian nucleotide excision repair. Nat. Cell Biol. *8,* 640-642.

Ogi, T., Limsirichaikul, S., Overmeer, R.M., Volker, M., Takenaka, K., Cloney, R., Nakazawa, Y., Niimi, A., Miki, Y., Jaspers, N.G., et al. (2010). Three DNA polymerases, recruited by different mechanisms, carry out NER repair synthesis in human cells. Mol. Cell *37,* 714-727.

Olovnikov, A.M. (1973). A theory of marginotomy. The incomplete copying of template margin in enzymic synthesis of polynucleotides and biological significance of the phenomenon. J. Theor. Biol. *41,* 181-190.

Palm, W., and de Lange, T. (2008). How shelterin protects mammalian telomeres. Annu. Rev. Genet. *42*, 301-334.

Parikh, D., Fouquerel, E., Murphy, C.T., Wang, H., and Opresko, P. (2015). Telomeres are partly shielded from ultraviolet-induced damage and proficient for nucleotide excision repair of photoproducts. Ncomms. *6,* 8214.

Park, C.H., Mu, D., Reardon, J.T., and Sancar, A. (1995). The general transcription-repair factor TFIIH is recruited to the excision repair complex by the XPA protein independent of the TFIIE transcription factor. J. Biol. Chem. *270,* 4896-4902.

Pennock, E., Buckley, K., and Lundblad, V. (2001). Cdc13 deliver separate complexes to the telomere for end protection and replication. Cell *104,* 387-396.

Premkumar, V.L., Cranert, S., Linger, B.R., Morin, G.B., Minium, S., and Price, C. (2014). The 3` overhangs at *Tetrahymena thermophila* telomeres are packaged by four proteins, Pot1a, Tpt1, Pat1, and Pat 2. Eukaryot. Cell *13,* 240-245.

Puglisi, A., Bianchi, A., Lemmens, L., Damay, P., and Shore, D. (2008). Distinct roles for yeast Stn1 in telomere capping and telomerase inhibition. EMBO J. *27,* 2328-2339.

Ramírez, R., Carracedo, J., Jimenez, R., Canela, A., Herrera, E., Aljama, P., and Blasco, M.A. (2002). Massive telomere loss in an early event of DNA damage-induced apoptosis. J. Biol. Chem. *278,* 836-842.

Ramsey, K.L., Smith, J.J., Dasgupta, A., Maqani, N., Grant, P., and Auble, D.T. (2004) The NEF4 complex regulates Rad4 levels and utilizes Snf2/Swi2-relatd ATPase activity for nucleotide excision repair. Mol. Cell Biol. *24,* 6362-6378.

Riethman, H. (2008). Human telomere structure and biology. Annu. Rev. Genom. Hum. Genet. *9,* 1-19.

Robles-Espinoza, C.D., Harland, M., Ramsay, A.J., Aoude, L.G., Quesada, V., Ding, Z., Pooly, K.A. Pritchard, A.L., Tiffen, J.C. Petljak, M., et al. (2014). POT1 loss-of-function variants predispose to familial melanoma. Nat. Genet. *46,* 478-481.

Rochette, P.J., and Brash, D.E. (2010). Human telomeres are hypersentivie to UV-induced DNA damage and refractory to repair. PLOS Genet. *6,* e1000926.

Sambrook, J., and Russell, R.W. (2001) Molecular cloning: a laboratory manual, 3rd ed. Cold Spring Harbor Lab. Press.

Schärer, O.D. (2013). Nucleotide excision repair in eukaryotes. Cold Spring Harb. Perspect. Biol. *5,* a012609.

Scrima, A., Konickova, R., Czyzewski, B.K., Kawasaki, Y., Jeffrey, P.D., Groisman, R., Nakatani, Y., Iwai, S., Pavletich, N.P., and Thoma, N.H. (2008). Structural basis of UV DNA-damage recognition by the DDB1-DDB2 complex. Cell *135,* 1213-1223.

Shampay, J., Szostak, J.W., and Blackburn, E.H. (1984). DNA sequences of telomeres maintained in yeast. Nature *305,* 189-193.

Shippen-Lentz, D., and Blackburn, E.H. (1990). Functional evidence for an RNA template in telomerase. Science. *247,* 546-552.

Stout, G.J., and Blasco, M.A. (2013). Telomere length and telomerase activity impact the UV sensitivity syndrome Xeroderma Pigmentosum C. Cancer Res. *73,* 1844-1854.

Stanley, S.E., Chen, J.J., Podlevsky, J.D., Alder, J.K. Handel, N.N., Mathias, R.A., Qi, X., Rafaels, N.M., Wise, R.A., Silverman, E.K., et al. (2015). Telomerase mutations in smokers with severe emphysema. J. Clin. Invest. *125,* 563-570.

Stewart, J.A., Chaiken, M.F., Wang, F., and Price, C.M. (2012). Maintaining the end: roles of telomere proteins in end-protection, telomere replication and length regulation. Mutat. Res. *730,* 12-19.

Stover, N.A., Punia, R.S., Bowen, M.S., Dolins, S.B., and Clark, T.G. (2012). Tetrahymena Genome Database Wiki: a community-maintained model organism database. Database (Oxford). *20,* bas007.

Sugasawa, K., Okamoto, T., Shimizu, Y., Masutani, C., Iwai, S., and Hanaoka, F. (2001). A multistep damage recognition mechanism for global genomic nucleotide excision repair. Genes Dev. *15,* 507-521.

Sugasawa, K., Akagi, J., Nishi, R., Iwai, S., and Hanaoka, F. (2009). Two-step recognition of DNA damage for mammalian nucleotide excision repair: directional binding of the XPC complex and DNA strand scanning. Mol. Cell *36,* 642-653.

Szostak, J.W. and Blackburn, E.H. (1982). Cloning yeast telomeres on linear plasmid vectors. Cell *29,* 245-255.

Szymkowski, D.E., Lawrence, C.W., and Wood, R.D. (1993). Repair by human cell extract of single (6-4) and cyclobutane thymine-thymine photoproducts in DNA. Proc. Natl.Acad. Sci. USA. *90*, 9823-9827.

Tang, J.Y., Hwang, B.J., Ford, J.M., Hanawalt, P.C., and Chu, G. (2000). Xeroderma pigmentosum p48 gene enhances global genomic repair and suppresses UV-induced mutagenesis. Mol. Cell *5,* 737-744.

Tapias, A., Auriol, J., Forget, D., Enzlin, J.H., Schärer, O.D., Coin, F., Coulombe, B., and Egly, J.M. (2004). Ordered conformational changes in damaged DNA induced by nucleotide excision repair factors. J. Biol. Chem. *279,* 19074-19083.

Ting, A.P.L., Low, G.K.M., Gopalakrishnan, K., and Hande, M.P. (2010). Telomere attrition and genomic instability in xeroderma pigmentosum type-b deficient fibroblasts under oxidative stress. J. Cell. Mol. Med. *14,* 403-416.

Tomita, K., and Cooper, J.P. (2008). Fission yeast Ccq1 is telomerase recruiter and local checkpoint controller. Genes Dev. *22,* 3461-3474.

Van Belle, G.J.C. (2015). Differential pathway control in nucleotide excision repair.

Volker, M., Mone, M.J., Karmakar, P., van Hoffen, A., Schul, W., Vermeulen, W., Hoeijmakers, J.H., van Driel, R., van Zeeland, A.A., and Mullenders, L.H. (2001). Sequential assembly of the nucleotide excision repair factors in vivo. Mol. Cell *8,* 213-224.

Wakasugi, M., and Sancar, A. (1998). Assembly, subunit composition, and footprint of human DNA repair excision nuclease. Proc. Natl. Acad. Sci. *95,* 6669-6674.

Wakasugi, M., Kasashima, H., Fukase, Y., Imura, M., Imai, R., Yamada, S., Cleaver, J.E., and Matsunaga, T. (2009). Physical and functional interaction between DDB and XPA in nucleotide excision repair. Nucleic Acids Res. *37,* 516-525.

Watson, J.D. and Crick, F.H.C. (1953). Molecular structure of nucleic acids. Nature *171,* 737-738.

Weeded, C.E. and Asselin-Labat, M.L. (2018). Mechanisms of DNA damage repair in adult stem cells and implications for cancer formation. Biochem. Biophys. Acta. *1864,* 89-101.

Wu, Y., Mitchell, T.R., and Zhu, X.D. (2008). Human XPF controls TRF2 and telomere length maintenance through distinctive mechanisms. Mech. Ageing Dev. *129,* 602-610.

Xin, H., Liu, D., Wan, M., Safari, A., Kim, H., Sun, W., O'Connor, M.S., and Songyang, Z. (2007). TPP1 is a homologue of ciliate TEBP-beta and interacts with POT1 to recruit telomerase. Nature *445,* 559-562.

Yao, M.C., Blackburn, E., and Gall, J.G. (1979). Amplification of the rRNA genes in Tetrahymena. Quant. Biol. *43*, 1293–1296.

Yao, M.C., Blackburn, E., and Gall, J. (1981) Tandemly repeated C-C-C-C-A-A hexanucleotide of Tetrahymena rDNA is present elsewhere in the genome and may be related to the alteration of the somatic genome. J. Cell Biol. *90*, 515–520.

Ye, J.Z., Hockemeyer, D., Krutchinsky, A.N., Loayaz, D., Hooper, S.M. Chait, B.T., and de Lange, T. (2004). POT1-interacting protein PIP1: a telomere length regulator that recruits POT1 to the TIN2/TRF1 complex. Genes Dev. *18,* 1649-1654.

Zhu, X.D., Niedernhofer, B.K. Mann, M., Hoeijmakers, J., and de Lange, T. (2003). ERCC1/XPF removes the 3` overhang from uncapped telomeres and represses formation of telomeric DNA-containing double minute chromosomes. Mol. Cell*12,* 1489-1496.